A nucleoside signal generated by a fungal endophyte regulates host cell death and promotes root colonization

Nick Dunken[1], Heidi Widmer[1], Gerd U. Balcke[2], Henryk Straube[3,4], Gregor Langen[1,5], Nyasha M. Charura[1], Pia Saake[1,5], Concetta De Quattro[1,5], Jonas Schön[6], Hanna Rövenich[1,5], Stephan Wawra[1,5], Armin Djamei[7], Matias D. Zurbriggen[6], Alain Tissier[2], Claus-Peter Witte[3] and Alga Zuccaro[1,5*]

[1] University of Cologne, Institute for Plant Sciences, Cologne, Germany

[2] Department of Cell and Metabolic Biology, Institute of Plant Biochemistry, Halle (Saale), Germany

[3] Department of Molecular Nutrition and Biochemistry of Plants, Institute of Plant Nutrition, Leibniz University Hannover, Hannover, Germany

[4] Faculty of Science, Department of Plant and Environmental Sciences, Section for Plant Biochemistry, University of Copenhagen, Copenhagen, Denmark

[5] Cluster of Excellence on Plant Sciences (CEPLAS), Germany

[6] Institute of Synthetic Biology and CEPLAS, Heinrich-Heine-University Düsseldorf[6], Germany

[7] Department of Plant Pathology, Institute of Crop Science and Resource Conservation (INRES), University of Bonn, Bonn, Germany

[*] Corresponding author: azuccaro@uni-koeln.de

Summary

The intracellular colonization of plant roots by the beneficial fungal endophyte *Serendipita indica* follows a biphasic strategy. After an early biotrophic phase, the interaction transitions to a host cell death phase restricted to the epidermal and cortex layers of the root. Host cell death contributes to the successful accommodation of the fungus during the beneficial interaction in *Arabidopsis thaliana*. How host cell death is initiated and controlled is largely unknown. Here we show that two fungal enzymes, the ecto-5'-nucleotidase *Si*E5NT and the nuclease *Si*NucA, act synergistically in the plant apoplast at the onset of cell death to produce deoxyadenosine (dAdo), a potent cell death inducer in animal systems. The uptake of extracellular dAdo, but not the structurally related adenosine (Ado), activates a previously undescribed cell death mechanism in *A. thaliana*. Mutation of the equilibrative nucleoside transporter ENT3 in *A. thaliana* results in resistance to cell death triggered by extracellular dAdo and reduced fungal-mediated cell death during root colonization. A library screen of *A. thaliana* T-DNA insertion lines identified a toll/interleukin-1 receptor nucleotide-binding leucine-rich repeat (TIR-NLR) protein as an additional intracellular component in dAdo-triggered cell death. Mutation of this previously uncharacterised TIR-NLR, which we have

named ISI (induced by *S. indica*), affects host cell death, fungal colonization and growth promotion, suggesting a key role in the regulation of root cell death and plant-microbe interaction. Our data show that the combined activity of two fungal apoplastic enzymes leads to the production of a metabolite that, upon uptake, triggers TIR-NLR-modulated plant cell death, providing a link to immunometabolism in plants.

Short summary

Efficient intraradical colonization by the beneficial fungal endophyte *Serendipita indica* requires restricted host cell death. How this symbiotic host cell death is initiated and controlled is largely unknown. Here we show that two fungal enzymes, the ecto-5'-nucleotidase *Si*E5NT and the nuclease *Si*NucA, act synergistically in the apoplast at the onset of cell death to produce deoxyadenosine (dAdo), a potent cell death inducer in animal systems. Uptake of extracellular dAdo activates a previously undescribed cell death mechanism in plants. Mutation of the *A. thaliana* equilibrative nucleoside transporter *ENT3* leads to resistance to cell death triggered by uptake of extracellular dAdo and to reduced fungal-mediated cell death during colonization. A library screen of *A. thaliana* T-DNA insertion lines identified a TIR-NLR protein as an additional intracellular component in dAdo-triggered cell death, providing a link to immunometabolism in plants.

In a nutshell

Regulated host cell death is part of the plant defense strategy against pathogens, but it is also involved in the accommodation of certain beneficial microbes in the roots. We have identified extracellular metabolites and intracellular metabolic signals that contribute to colonization by beneficial root fungal endophytes and uncovered a conserved cell death mechanism likely co-opted for establishing plant-endophyte symbiosis.

Introduction

Regulated cell death (RCD) occurs in plants as part of normal growth and development and in response to abiotic and biotic stimuli. In plant-microbe interactions, host cell death programs can mediate either resistance or successful infection. Depending on the type of microbial lifestyle (biotrophic or necrotrophic), host cell death can benefit the plant by stopping the growth of biotrophs, or the microbe by promoting the growth of necrotrophs. Thus, control of plant host cell death is critical to the outcome of an interaction. Host cell death also plays a critical role in certain beneficial interactions, challenging the paradigm that cell death in plant-microbe interactions implies pathogenesis or host-microbe incompatibility. Both symbiosis with beneficial microbes and infection by pathogens require sophisticated control of host defenses and nutrient fluxes. Certain features of the interaction of beneficial microbes with plants, such as affecting host immunity, metabolism, and host cell death, are reminiscent of pathogen infections. In Rhizobium-legume symbioses, root nodules are formed to provide a niche for bacterial nitrogen fixation. The formation of infection pockets in some of these symbioses is associated with host cell death and the production of hydrogen peroxide (D'Haeze et al., 2003). Host cell death is also observed in

ectomycorrhizal symbioses (Mucha et al., 2014; Ragnelli et al., 2014) and is a requisite for the establishment of symbiotic interactions with the widely distributed beneficial fungi of the order Sebacinales (Deshmukh et al., 2006; Lahrmann et al., 2013; Qiang et al., 2012). Molecular environmental studies have shown that some of the most abundant taxa of this order have little, if any, host specificity and interact with a wide variety of plant species. Sebacinales isolates, including *S. indica* and *S. vermifera*, exhibit beneficial effects such as growth promotion, increased seed production, and protection from pathogens, and thus play an important role in natural and managed ecosystems (Oberwinkler et al., 2013; Tedersoo et al., 2014; Weiss et al., 2016). The requirement of restricted host cell death for the establishment of certain beneficial microorganisms leads to the hypothesis that the activation of cell death mechanisms in roots has a more important ecological function than previously thought.

In the hosts *Hordeum vulgare* (hereafter barley) and *A. thaliana* (hereafter Arabidopsis), fungi of the order Sebacinales initially colonize living cells that die during the progression of colonization (Deshmukh *et al.*, 2006; Lahrmann *et al.*, 2013; Lahrmann et al., 2015; Lahrmann and Zuccaro, 2012; Qiang *et al.*, 2012; Zuccaro et al., 2011). This symbiotic cell death is thought to contribute to niche differentiation during microbial competition for space and nutrients in the root and appears to be restricted to colonized cells in the epidermis and outer cortex. The host pathways that control the induction and execution of plant cell death and the fungal elicitors/effectors that initiate this process in roots are still largely unknown (Lahrmann *et al.*, 2013; Nizam et al., 2019; Qiang *et al.*, 2012; Schneider and Lynch, 2018). Pathogenic and beneficial fungi have a large repertoire of secreted effectors that can affect host cell physiology and suppress plant defenses, promoting fungal colonization. In fungi, effectors have been described mainly in biotrophic and hemibiotrophic foliar pathogens (Lo Presti et al., 2015). In contrast, only a few effectors of root symbiotic fungi have been functionally characterized (Kloppholz et al., 2011; Nizam *et al.*, 2019; Nostadt et al., 2020; Plett et al., 2014; Voß et al., 2018; Wawra et al., 2016). Therefore, the modes of action of effectors of mutualistic fungi remain poorly understood.

Using genomics, transcriptomics, and proteomics, we identified proteins secreted by *S. indica* in the root apoplast, the space outside the plasma membrane, including cell walls, where material can freely diffuse (Nizam *et al.*, 2019). One secreted fungal protein consistently found at various stages of symbiosis is the ecto-5'-nucleotidase *Si*E5NT (PIIN_01005) (Nizam *et al.*, 2019). Expression of *SiE5NT is* induced during colonization of barley and Arabidopsis roots, but not in axenic fungal culture (Nizam *et al.*, 2019). Animal ecto-5'-nucleotidases play a key role in the conversion of AMP to adenosine, counteracting the immunogenic effects of extracellular adenosine 5'-triphosphate (eATP) released from stimulated host cells (Antonioli et al., 2013). Extracellular ATP is an important signaling molecule in plants that controls development and response to biotic and abiotic stresses. In Arabidopsis, eATP mediates various cellular processes through its binding to the purinergic membrane-associated receptor proteins DORN1/P2K1 and the recently described P2K2 (Pham et al., 2020). In the apoplast, ATP accumulation increases cytoplasmic calcium and triggers a defense response against invading microbes. The perception of extracellular

117 nucleotides, such as eATP, plays an important role in plant-fungal interactions – we recently
118 demonstrated this by colonization experiments with the knockout (KO) mutant *dorn1* of
119 Arabidopsis, which is better colonized by *S. indica*. *Si*E5NT is able to hydrolyze ATP, ADP,
120 and AMP to adenosine and phosphate, which alters the eATP content in the apoplast and
121 the plant response to fungal colonization (Nizam et al., 2019). Secretion of *Si*E5NT in
122 Arabidopsis leads to enhanced colonization by *S. indica*, confirming its role as an apoplastic
123 effector protein. Considering the important role *Si*E5NT plays in fungal accommodation at
124 early symbiotic stages, we proposed that modulation of extracellular nucleotide levels and
125 their perception play a key role in compatibility during early plant-fungal interactions in roots
126 (Nizam *et al.*, 2019). Secreted *Si*E5NT homologs are also present in fungal pathogens such
127 as *Colletotrichium incanum* and *Fusarium oxysporum* and other Arabidopsis endophytes
128 such as *Colletotrichum tofieldiae*, where their expression is induced during colonization,
129 suggesting that purine-based extracellular biomolecules also play a role in other plant-
130 fungal interactions.

131 At the onset of cell death, a small fungal endonuclease, which we named *Si*NucA
132 (PIIN_02121), is secreted simultaneously with *Si*E5NT during colonization of barley and
133 Arabidopsis by *S. indica* (Nizam *et al.*, 2019; Thürich et al., 2018). In plants, the mechanisms
134 linking immune recognition of DNA danger signals in the extracellular environment to innate
135 signaling pathways in the cytosol are poorly understood, as is the role of (deoxy)nucleotide
136 metabolism in root colonization and cell death. Here we show that the synergistic activity of
137 *Si*NucA and *Si*E5NT leads to the production of deoxyadenosine (dAdo) and, in smaller
138 amounts, other deoxynucleosides from extracellular DNA (eDNA). eDNA can be released
139 from roots during microbial colonization in a process called root extracellular trap (RET)
140 formation, or from dying cells and from microorganisms during biofilm development on the
141 root surface (Chambard et al., 2021; Driouich et al., 2019; Tran et al., 2016; Wen et al.,
142 2009). The production of dAdo by fungal extracellular enzymes is similar to the processes
143 involved in dAdo-mediated immune cell death of *Staphylococcus aureus* in animals, which
144 appears to ensure bacterial survival in host tissues (Thammavongsa et al., 2013; Winstel et
145 al., 2018). Staphylococcal nuclease and adenosine synthase A (AdsA, a homolog of
146 *Si*E5NT) are both required to release dAdo from neutrophil extracellular traps (NETs), which
147 has a potent cytotoxic effect on macrophages and other immune cells (Thammavongsa *et*
148 *al.*, 2013).
149 Here we show that extracellular dAdo, but not the structurally similar Ado, activates a
150 previously unidentified cell death mechanism in plants. Expression of either extracellular
151 *Si*NucA or *Si*E5NT *in planta* results in enhanced colonization by *S. indica* and host cell death
152 (Nizam *et al.*, 2019). We found that a mutation in the equilibrative nucleoside transporter 3
153 (ENT3) of Arabidopsis leads to a strong resistance phenotype to dAdo-induced cell death
154 but not to methyl jasmonate, a cell death inducer of senescence. Accordingly, compared
155 with the WT line colonized by *S. indica,* the *ent3* KO line shows less fungal-induced cell
156 death in the root and accumulates less of the extracellular signaling metabolite
157 methylerythritol cyclodiphosphate (MEcPP) in response to fungal colonization or dAdo
158 treatment. Finally, in a mutant screen of Arabidopsis T-DNA insertion lines, we found that a
159 previously uncharacterized TIR-NLR protein is involved in modulating cell death triggered

160 by dAdo as well as fungal colonization and growth promotion. Most characterized TIR-NLRs
161 (TNLs) act as sensors of effectors secreted by pathogens. The involvement of a TNL protein
162 in the modulation of cell death by a symbiotically produced metabolite establishes a
163 connection to immunometabolism in plants. Therefore, we propose that hydrolysis of
164 extracellular metabolites by the fungal-derived *Si*NucA and *Si*E5NT provides a direct link
165 between purine metabolism, immunity, and cell death programs in roots (Figure 1).

166 **Results**

167 **Fading of host nuclei and vacuolar collapse are hallmarks of symbiotic cell death**
168 **during *S. indica* root colonization**

169 *S. indica* induces restricted cell death in colonized root cells of Arabidopsis and barley,
170 resulting in characteristic cytological features at later stages of colonization. In these two
171 hosts, the timing and extent of cell death differs (Lahrmann *et al.*, 2013; Qiang *et al.*, 2012).
172 In Arabidopsis, the cell death phenotype is less pronounced than in barley, but cytological
173 analyses showed fading of host nuclei, vacuolar collapse (Figure 2A-M), and swelling of the
174 endoplasmic reticulum (ER) in colonized cells (Qiang *et al.*, 2012) indicating ER stress and
175 host cell death during root colonization. To characterize the timing of fungal-induced cell
176 death, the presence and shape of plant nuclei during colonization by *S. indica* were
177 monitored by confocal laser scanning microscopy using either the nucleic acid dye DAPI
178 (4',6-diamidino-2'-phenylindole dihydrochloride) and the cell death dye SYTOX Orange
179 (Figure 2C-I) or an Arabidopsis line expressing the nuclear marker H2B:mCherry (Figure
180 2A, B). Nuclei stained with SYTOX Orange were visible 7 to 8 days post inoculation (dpi),
181 indicating that at this time the plasma and nuclear membranes of Arabidopsis were
182 permeable to the dye, which is a hallmark of cell death (Figure 2F, G). In the Arabidopsis
183 H2B:mCherry line, plant nuclei in the epidermal layer were often elongated, faded, and
184 eventually disappeared by 8 to 10 dpi in heavily colonized areas of the root (Figure 2A, B).
185 In dying cells, *S. indica* hyphae embedded in plant nuclei were frequently observed,
186 indicating that the fungus can digest and feed on host nuclear DNA (Figure 2C-E, H, I).
187 Cytological analyses show that Arabidopsis root cell death begins around 7 dpi and by 10
188 dpi most host nuclei have faded or disappeared in cells colonized by *S. indica* under the
189 growth condition tested.

190 ***Si*NucA and *Si*E5NT act synergistically in the production of deoxynucleosides**

191 Although the interaction between *S. indica* and plant roots has been extensively studied,
192 comparatively little is known about the contribution of apoplastic effectors to fungal
193 accommodation or the mechanism of cell death in this system (Nizam *et al.*, 2019; Nostadt
194 *et al.*, 2020; Rafiqi et al., 2013; Wawra *et al.*, 2016). We previously analyzed soluble
195 apoplastic proteins in barley at different stages of *S. indica* colonization. We found that
196 *Si*E5NT was one of the predominant fungal proteins consistently present in this extracellular
197 compartment (Nizam *et al.*, 2019). We demonstrated that *Si*E5NT functions as a membrane-
198 bound nucleotidase that is released into the apoplast during host colonization. *Si*E5NT is
199 capable of releasing phosphate and adenosine from ATP, ADP, and AMP (Nizam *et al.*,

200 2019). In addition, the small secreted protein *Si*NucA with predicted endonuclease activity
201 (Figure S1) was found in the apoplastic fluid of colonized barley roots at the onset of cell
202 death (5 dpi) (Nizam *et al.*, 2019). *Si*NucA is also secreted during root colonization in
203 Arabidopsis (Thürich *et al.*, 2018). *Si*NucA expression is transiently induced during cell
204 death in barley and Arabidopsis compared with axenic fungal growth, as shown by
205 transcriptomic data (Lahrmann *et al.*, 2013) and quantitative PCR analyses (Figure 3A).
206 This prompted us to further investigate the involvement of this small secreted protein in
207 fungal colonization and host cell death. The secretion of *Si*NucA and its enzymatic activity
208 were investigated by overexpressing a *SiNucA*:HA:His construct in *S. indica* (Figure 3B,
209 S2). Supernatants from fungal OE strains, but not from empty vector control strains, and
210 affinity-purified *Si*NucA were able to degrade single- and double-stranded DNA and RNA
211 from fungal and plant material, indicating nonspecific nuclease activity (Figure 3C). Addition
212 of magnesium and calcium increased *Si*NucA activity in *in vitro* assays, whereas EDTA
213 inhibited it (Figure S3).

214 To investigate the effects of *Si*NucA on colonization, we tested independent homozygous
215 T3 lines heterologously expressing a native version of *SiNucA* in Arabidopsis under control
216 of the 35S promoter. As controls, we used WT and segregating lines lacking the *SiNucA*
217 gene. Expression of *SiNucA* in Arabidopsis resulted in higher fungal colonization at 7 dpi,
218 which correlated with the *SiNucA* expression level (Figure 3D, E), demonstrating its
219 importance in fungal accommodation. Overcolonization resulted in a reduction in plant
220 biomass that was not observed in the mock-treated *SiNucA* expression lines (Figure S4).
221 Localization studies by confocal microscopy of Arabidopsis roots expressing either full-
222 length *Si*NucA or a version lacking the N-terminal signal peptide (SP) fused to mCherry
223 confirmed secretion of the full-length *Si*NucA fusion protein into the apoplast and
224 functionality of the SP. After plasmolysis with 1M NaCl or sorbitol, the mCherry fluorescence
225 signal was visible on the cell walls and apparently on the membrane of the shrinking cells
226 for the full-length *Si*NucA fusion protein, but not for the cytoplasmic version without SP
227 (Figure S5). Remarkably, the presence of *S. indica* resulted in relocalization of the full-length
228 mCherry-tagged *Si*NucA to host nuclei only in cells colonized by the fungus and not in
229 bystander cells, where the mCherry signal remained at the cell periphery even after
230 plasmolysis (Figure 3F and S5, S6). The presence of *Si*NucA in the apoplast (Nizam *et al.*,
231 2019) and in the nucleus of colonized host cells (Figure 3F) suggests that this small secreted
232 protein can be redirected to the nucleus during colonization and can act on both eDNA and
233 nuclear DNA.

234 The co-occurrence of *Si*NucA and *Si*E5NT in the apoplast at 5 dpi led us to speculate that
235 these two enzymes might cooperate in promoting fungal colonization of roots. Using *Si*E5NT
236 affinity-purified from leaves of *Nicotiana benthamiana* that transiently expressed the
237 enzyme as a secreted C-terminal Strep-tagged variant, we found activity with dAMP and
238 AMP (Figure 4A), whereas no activity was detected for other deoxyribonucleotides (dGMP,
239 dCMP, dTMP) or ribonucleotides (GMP, UMP, 3′,5′-cAMP) tested. Moreover, dATP and the
240 general phosphatase substrate *para*-nitrophenyl pyrophosphate (*p*NPP) were not *Si*E5NT
241 substrates. Interestingly, only dAMP was hydrolyzed at a constant rate, whereas the AMP

242 hydrolysis rate gradually decreased under the selected reaction conditions (Figure S7A, B).
243 The K_M for AMP (15.9 µM) was ~20-fold lower than for dAMP (361.6 µM), but the k_{cat} for
244 dAMP (11.9 s^{-1}) exceeded that of AMP (1.1 s^{-1}) by a factor of ~10 (Figure 4A, B). These
245 data suggest that *Si*E5NT hydrolyzes AMP slightly better at low substrate concentrations
246 (below 20 µM), but is far more efficient for dAMP at higher substrate concentrations that
247 might prevail in a nucleus undergoing degradation and in the case of eDNA degradation.
248 To test the ability of *Si*NucA and *Si*E5NT to work together, we incubated DNA with *Si*E5NT
249 and *Si*NucA alone and in combination. As expected, *Si*NucA alone degraded DNA (Figure
250 4C), but neither deoxyribonucleotides nor deoxynucleosides were detected as reaction
251 products by LC-MS analysis, suggesting that *Si*NucA degrades DNA to oligonucleotides.
252 *Si*E5NT alone also did not release deoxyribonucleotides from DNA, but produced small
253 amounts of deoxyribonucleosides (Figure 4D). However, in combination, *Si*NucA and
254 *Si*E5NT released deoxyribonucleosides from DNA with a strong preference for dAdo. This
255 demonstrates the ability of *Si*E5NT to use oligonucleotides released by *Si*NucA as a
256 substrate and act synergistically with *Si*NucA to preferentially release dAdo from DNA
257 (Figure S7C).

258 **dAdo induces host cell death**

259 The production of dAdo by the synergistic activity of the two secreted fungal enzymes
260 resembles the processes involved in dAdo-mediated immune cell death of *Staphylococcus*
261 *aureus* in animal cells, which ensures the exclusion of macrophages from the center of
262 abscesses where the bacteria survive (Thammavongsa *et al.*, 2013; Winstel *et al.*, 2018).
263 This motivated us to test the effect of dAdo in plants. Incubation of the H2B-mCherry line of
264 Arabidopsis with extracellular dAdo, but not with Ado or buffer, resulted in the fading and
265 disappearance of nuclei in roots within 48 hours (Figure 5A). This root cell death phenotype
266 could be quantified using Evans blue azo dye (Figure 5B, C). In addition, extracellular dAdo-
267 triggered hallmarks of cell death, such as increased electrolyte leakage, induction of cell
268 death marker gene expression as well as activation of the 26S proteasome and decreased
269 photosynthetic activity (F_V/F_M) (Figure 5D-H, S8). The effects were concentration-
270 dependent, and removal of dAdo from the culture supernatant 24 hours after treatment
271 resulted in recovery of Arabidopsis seedlings, indicating that activation of the cell death
272 program in Arabidopsis is still reversible at this stage (Figure S9, S10).

273 A cell death phenotype was also observed in young leaves of *N. benthamiana* during
274 expression by *Agrobacterium tumefaciens* infiltration of a full length *Si*E5NT construct with
275 the signal peptide for secretion into the apoplastic space (Figure S11, S12) and in seedlings
276 incubated with dAdo (Figure S13). Cell death was not visible in older leaves or in leaves of
277 *N. benthamiana* expressing the control vector p19 or *Si*NucA alone. The observed
278 phenotype suggests that the presence of *Si*E5NT is sufficient to trigger cell death in this
279 plant host upon wounding/damage by agroinfiltration, which could release DNA and
280 DNAses into the apoplast or elicit a response to the presence of the bacterium or its proteins
281 (Figure S11, S12). To test whether cell death triggered by dAdo is conserved in basal plant
282 lineages, we additionally tested its activity in the liverwort *Marchantia polymorpha*.

283 Incubation with dAdo also induced cell death in this plant species (Figure S14). Overall,
284 these data suggest that the dAdo-mediated cell death mechanism is conserved across plant
285 lineages.

286 **dAdo induces the MEP pathway and accumulation of the stress signaling metabolite**
287 **MEcPP**

288 To investigate the mechanism by which dAdo triggers cell death in plants and to determine
289 whether it activates stress signaling pathways, we analyzed the transcriptional response of
290 Arabidopsis to this metabolite at 0, 3, and 12 h compared to a buffer control using RNA-
291 seq. Most marker genes for regulated cell death (Olvera-Carrillo et al., 2015) were
292 upregulated at 12 hours (Figure 5I & Table S1-3). In addition, the plastidial 2-C-methyl-D-
293 erythritol-4-phosphate (MEP) pathway was induced upon incubation with dAdo after 12
294 hours in Arabidopsis seedlings (Figure 5J & Table S4). Accordingly, MEcPP, a precursor of
295 plastidial isoprenoids and a stress-specific retrograde signaling metabolite produced by the
296 MEP pathway, accumulated extracellularly 3 days after treatment as measured by LC-
297 MS/MS (Figure 5J). Abiotic stress and wounding increase levels of cytoplasmic MEcPP,
298 which coordinates stress response pathways in plants (Xiao et al., 2012). The detection of
299 this isoprenoid intermediate in the extracellular environment after dAdo treatment suggests
300 that this metabolite may serve as a stress signal in bystander cells, a putative important
301 function that needs further investigation. Incubation of Arabidopsis with extracellular MEcPP
302 did not result in cell death, demonstrating that accumulation of this metabolite is not
303 sufficient to trigger cell death and therefore is not the cause of the observed dAdo-mediated
304 cell death (Figure S15).

305 **dAdo-triggered signaling and cell death are not mediated by canonical pattern-**
306 **triggered immune responses**

307 To determine whether cell death triggered by dAdo is mediated by signals generated by an
308 immune receptor at the cell surface, we tested the ability of this metabolite to trigger a rapid
309 response by monitoring calcium influx and ROS production. Both responses are part of PTI
310 (pattern-triggered immunity), a process activated by recognition of MAMPs (microbe-
311 associated molecular patterns) or DAMPs (damage-associated molecular patterns) by
312 pattern-recognition receptors (PRRs) at the plasma membrane (Ngou et al., 2021; Yuan et
313 al., 2021; Zipfel and Oldroyd, 2017).

314 Incubation of Arabidopsis seedlings with dAdo did not elicit calcium influx, whereas
315 treatment with ATP or ADP, which have been previously described as DAMPs (Choi et al.
316 2014; Tanaka et al. 2014) but also with dATP or dADP triggered a rapid calcium influx that
317 was dependent on the extracellular ATP receptor DORN1 (Figure 6 A-C). Treatment with
318 dAdo or with any of the other purine derivatives did not induce a ROS burst (Figure S16).
319 On the other hand, incubation with dAdo and to a lesser extent with ATP or dAMP, but not
320 Ado, resulted in accumulation of the marker metabolite MEcPP and induction of the
321 DAMP/MAMP- and fungus-responsive gene AT1G58420 at 3 dpt (Figure 6D, E & Table S5)
322 (Choi et al., 2014; Kilian et al., 2007; Nizam *et al.*, 2019). Overall, these data suggest that

323 dAdo does not act as a typical extracellular DAMP or MAMP but induces a signaling
324 pathway independent of calcium influx and ROS production.

325 **The Arabidopsis transporter ENT3 is required for dAdo-mediated signaling and cell**
326 **death**

327 The fact that we did not observe a canonical PTI response to dAdo led us to speculate that
328 uptake of this metabolite is necessary to promote plant signaling and trigger cell death. In
329 the animal system, treatment with extracellular dAdo leads to the accumulation of
330 intracellular dATP, which appears to impair DNA synthesis and induces apoptosis via
331 activation of caspase 3 (Winstel *et al.*, 2018). Rapidly dividing cells are particularly
332 susceptible to cell death triggered by dAdo and it has been shown that the toxic effect of
333 dAdo in the animal system depends on dAdo uptake by the human equilibrative nucleoside
334 transporter 1 (hENT1) (Winstel *et al.*, 2018). Similiarly, we observed high sensitivity of
335 dividing cells in root tips using Evans blue staining and young *N. benthamiana* plants (Figure
336 5 A,B; S11-13). On the contrary, *S. indica* was not sensitive to dAdo and showed normal
337 growth ratio even at high concentrations (Figure S17). In Arabidopsis, eight potential ENT
338 family members are annotated in the genome. Two of them are expressed in roots, namely
339 ENT3, which is localized at the plasma membrane, and ENT1, which is localized at the
340 tonoplast. The Arabidopsis KO line *ent3* showed a strong resistance phenotype to dAdo-
341 induced cell death compared with WT and *ent1* KO but is unaffected in the response to
342 methyl jasmonate-induced cell death (positive control) (Figure 7 A-C; S18). ENT3 has been
343 shown to transport adenosine and uridine with high affinity and to be inhibited in competitive
344 experiments by a number of different purine and pyrimidine nucleosides and 2'-
345 deoxynucleosides, including dAdo (Li et al., 2003). This suggests that ENT3 has a broad
346 substrate specificity and is a strong candidate for uptake of extracellular dAdo. In a
347 competition assay, addition of extracellular Ado decreased the cell death phenotype
348 induced by dAdo, suggesting that these two extracellular metabolites compete for the same
349 transporter at the cell membrane (Figure 7D). Interestingly, *ENT3* is more highly expressed
350 in the epidermis than in the rest of the root (Rich-Griffin et al., 2020), suggesting that dAdo-
351 induced cell death may be cell type specific to some extent. This is consistent with the
352 phenotype of root cell death observed after dAdo treatment with Evans blue staining (Figure
353 5B, C). Taken together, these data indicate that a functional ENT3 plays an important role
354 in dAdo-triggered cell death in Arabidopsis, most likely by importing dAdo into the
355 cytoplasm, where it activates signaling leading to cell death. Accordingly, the *ent3* KO line
356 accumulates lower levels of extracellular signaling metabolites such as MEcPP, GSSG, and
357 3′,5′-cAMP in response to dAdo treatment at 3 dpt compared with the WT line (Figure
358 7E,Table S6).

359 **Mutation of *ENT3* impairs *S. indica*-mediated cell death**

360 Next, we investigated whether ENT3 plays *a* role in fungal accommodation and cell death
361 mediated by *S. indica* in roots. The *ent3* KO Arabidopsis line showed significantly less cell
362 death upon colonization by *S. indica* compared with the WT line at 7, 10, and 14 dpi (Figure

363 7G, H). In addition, we observed a transient effect on fungal colonization at 8 dpi, where the
364 *ent3* KO line was less colonized by *S. indica* compared with the WT control, as determined
365 by qRT-PCR (Figure S19).

366 After colonization with *S. indica,* we also observed a transient accumulation of the
367 extracellular signaling metabolites 3′,5′-cAMP at 3 dpi (early biotrophic phase) and MEcPP
368 at 6 dpi (onset of cell death). In addition, a higher level of free phosphate was observed at
369 10 dpi (Figure 7F, Table S6). Consistent with the decreased cell death phenotype in the
370 *ent3* KO line, the amount of these metabolites was lower in this line when colonized by *S.*
371 *indica* compared with the WT line, suggesting that ENT3 is important for fungal-mediated
372 signal transduction and cell death in Arabidopsis. Modification of extracellular metabolites
373 levels by the activity of the fungal-derived enzymes *Si*NucA and *Si*E5NT and the host
374 transporter ENT3 provides, for the first time, a direct link between purine metabolism,
375 immunity, and cell death in roots. How the metabolic state of the host affects *S. indica*-
376 induced cell death remains to be thoroughly elucidated.

377 **A TIR-NLR protein is involved in dAdo-mediated cell death**

378 To identify downstream genetic determinants associated with dAdo-mediated cell death in
379 plants, we performed a mutant screen of 6868 SALK-Arabidopsis T-DNA insertion lines
380 (Figure S20). Sensitivity to dAdo was tested using Arabidopsis Col-0 WT as control and the
381 SALK mutant lines grown for 14 days on solid media (1/2 MS) in 24-well plates with and
382 without 500 µM dAdo. The dAdo-insensitive lines (survivors) from the screening were then
383 analyzed by PAM fluorometry in three independent biological replicates together with the
384 Col-0 WT line as control. Thirteen lines with varying degrees of dAdo resistance were
385 identified (Table S7). One of the resistant SALK lines had a mutation at the AT5G45240
386 locus (SALK_034517C), which encodes a predicted TIR domain nucleotide-binding,
387 leucine-rich repeat receptor (TIR-NLR). Mutation in this gene resulted in reproducible and
388 significantly high resistance to dAdo-induced cell death, as evidenced by reduced
389 electrolyte leakage, higher photosynthetic activity, and increased germination rate
390 compared to wild-type Col-0 after incubation with dAdo (Figure 8A-F). Complementation by
391 a cell-based transient expression system with the full-length TIR domain restored sensitivity
392 to dAdo in a concentration-dependent manner, suggesting that the TIR domain is involved
393 in mediating dAdo-induced cell death in Arabidopsis (Figure 8E). The TIR-NLR gene
394 AT5G45240 is located in close proximity to *RPS4* and *RRS1* and is part of a larger locus
395 containing multiple TNLs genes, most of which are functionally uncharacterized (Figure
396 S21). Four of the five TNLs genes at this locus showed transiently increased expression
397 during cell death associated with colonization by *S. indica*, with the AT5G45240 gene
398 displaying the strongest relative induction (Figure S22). We therefore named this gene ISI,
399 induced by *S. indica*. Induction could be detected especially during the onset of the cell
400 death-associated phase (Figure 9A). While the *isi* KO line showed less cell death after dAdo
401 treatment (Figure S23), there was increased cell death in the older parts of the mock-treated
402 roots and during colonization with *S. indica* compared to the WT line (Figure 9B), which
403 correlated with significantly greater fungal colonization (Figure 9C).. In addition, colonized

404 *isi* KO seedlings did not show *S. indica*-mediated promotion of root growth, as observed in
405 WT and *ent3* seedlings (Figure 9D and S24). These results could be explained by the
406 activation of an alternative cell death pathway in the absence of a functional ISI TIR-NLR,
407 leading to over-colonization by *S. indica* and loss of growth promotion (Figure 9E). Overall,
408 our data suggest that the ISI TIR-NLR protein is involved in modulating different cell death
409 programs in roots and mediating *S. indica* growth promotion. We further analysed the
410 expression of both TIR- and CC-NLRs in the roots of Arabidopsis during *S. indica*
411 colonization using RNA-seq data from different time points. We detected an induction of
412 expression for *ISI* and also for previously functionally characterized NLRs such as *ZAR1*
413 during beneficial colonization (Figure 9F and S25). Overall, the role of a TIR-NLR in dAdo-
414 induced cell death suggests that this cell death is regulated by the plant immune response
415 and is not a consequence of cytoplasmic toxicity, as assumed for animal cells.

416 **Discussion**

417 **Symbiotic cell death: an evolutionarily conserved mechanism?**

418 Root colonization by *S. indica* is associated with restricted host cell death. The mechanisms
419 behind the induction and regulation of this symbiotic cell death are poorly understood.
420 Previous work has shown that *S. indica* secretes *Si*E5NT, a ubiquitous apoplastic fungal
421 enzyme that catalyzes the conversion of adenosine nucleotides released from immune-
422 activated or damaged host tissues to adenosine (Nizam *et al.*, 2019). The mechanism of
423 the secreted ecto-5′-nucleotidase for host colonization appears to be similar to that evolved
424 by *S. aureus* and other animal pathogens to evade the host immune response by secreting
425 AdsA, which converts eATP to Ado, a suppressor of immunity in animal cells
426 (Thammavongsa et al., 2009). In addition to the release of eATP by damaged animal cells,
427 activated neutrophils release NETs, extracellular matrices composed of nuclear and
428 mitochondrial DNA and equipped with granular proteins, cell-specific proteases, and
429 antimicrobial peptides (Brinkmann et al., 2004). NETs rapidly immobilize and kill bacterial
430 pathogens (Driouich *et al.*, 2019). *S. aureus* escapes NETs by secreting proteases and the
431 nuclease Nuc, which degrade antimicrobial peptides and DNA. Nuclease-mediated
432 degradation of neutrophil NETs results in the formation of dAMP, which is converted to dAdo
433 by *S. aureus* AdsA. Macrophages and other immune cells are highly sensitive to dAdo
434 intoxication. This cellular intoxication is mediated by uptake via equilibrative nucleoside
435 transporters (Thammavongsa *et al.*, 2013; Winstel *et al.*, 2018). The escape mechanism of
436 *S. aureus* relies on the interaction of two extracellular microbial enzymes and allows
437 staphylococci to block infiltration of abscess lesions by phagocytes and elimination of the
438 bacteria. Similar to neutrophils, plant roots secrete RETs, extracellular root traps composed
439 of extracellular DNA and a variety of antimicrobial compounds and polysaccharides. RETs
440 and NETs share similar compositional and functional properties, but unlike NETs, RET
441 production is not triggered only upon microbial infection; instead, RETs are continuously
442 released during root development and form a large, mucus-rich network in the rhizosphere
443 (Chambard *et al.*, 2021; Driouich *et al.*, 2019; Hawes et al., 2016; Tran *et al.*, 2016). By
444 cytological analyses we observed that *S. indica* is able to grow within RETs and along the

445 root tip (Figure S26). The ability of *S. indica* to digest DNA *via* secretion of the nuclease
446 NucA, which accumulates in the root apoplast at the onset of cell death (Nizam *et al.*, 2019),
447 suggests the possibility of RET digestion by *S. indica* during colonization. Moreover,
448 localization of NucA in the nuclei of plant cells during S. indica colonization shows that this
449 enzyme is able to digest intracellular and extracellular DNA. Here, we show that the
450 combined enzymatic activity of *Si*E5NT and *Si*NucA, present simultaneously in the apoplast,
451 results in the conversion of oligonucleotides with terminal deoxyadenosine obtained by
452 nuclease digestion of DNA to free deoxyadenosine. Most importantly, we demonstrated that
453 uptake of deoxyadenosine via ENT3 is required for host cell death in roots. Mutation of
454 ENT3 results in reduced cell death during colonization by *S. indica*, demonstrating the
455 importance of extracellular nucleoside uptake in regulating fungal induced cell death. The
456 identification of a previously unknown immune-metabolic axis by which cells respond to
457 extracellular purine nucleosides and trigger cell death in plants suggests some conservation
458 or functional convergence between the immune avoidance and escape mechanisms
459 developed by *S. aureus* and other bacterial pathogens in animals and the cell death
460 triggered by dAdo during plant-fungal endophyte interactions in roots.

461 **A TIR-NLR regulates host cell death in roots**

462 To fight off infections by microbial pathogens, plants have evolved immune receptors that
463 are essential for a successful defense response. PRRs localized in the plasma membrane
464 are capable of sensing conserved MAMPs/DAMPs and eliciting a relatively mild PTI immune
465 response. Successful plant-associated microbes can provide a range of effectors to
466 attenuate PTI to enable successful host colonization. In turn, plants have evolved
467 polymorphic intracellular resistance proteins (R-proteins) to recognize the presence and/or
468 activity of effectors, resulting in a robust defense response called effector-triggered
469 immunity (ETI) that potentiates PTI (Ngou *et al.*, 2021; Yuan *et al.*, 2021). Most R proteins
470 belong to the nucleotide-binding (NB) leucine-rich repeat (LRR) family (NLR), which are
471 classified on the basis of their N-terminal domains as Toll-like interleukin 1 receptor (TIR)
472 type NLRs (TNLs) or coiled-coil type NLRs (CNLs) (Wu et al., 2019). TNLs generally
473 function as sensors for microbial effectors, whereas several CNLs are referred to as helper
474 NLRs and are downstream of many sensor NLRs in Arabidopsis (Saur et al., 2021; Wu *et*
475 *al.*, 2019). The involvement of the TNL ISI in resistance to dAdo-mediated cell death in
476 Arabidopsis suggests that this TIR-NLR might guard a protein targeted by dAdo.
477 Alternatively, it is possible that dAdo is converted to a plausible substrate of TNLs
478 associated with either nicotinamide adenine dinucleotide (NAD) or 2′,3′-cAMP, a
479 noncanonical cyclic nucleotide monophosphate (cNMP) (Horsefield et al., 2019; Wan et al.,
480 2019; Yu et al., 2021). Plant TIR domains of NLRs are enzymes that can degrade NAD in
481 its oxidized form (NAD^+). The NADase function of the TIR domain is necessary but not
482 sufficient to activate plant immune responses. Recently, it was shown that plant TIR proteins
483 are not only NADases but also act as 2′,3′-cAMP/cGMP synthetases by hydrolyzing
484 RNA/DNA. Mutations that specifically disrupt synthetase activity abolish TIR-mediated cell
485 death in *N. benthamiana,* demonstrating an important role for these cNMPs in TIR signaling.
486 (Yu *et al.*, 2021). The accumulation of extracellular 3′,5′-cAMP upon *S. indica* colonization

487 and treatment with dAdo establishes a link to cyclic nucleotide monophosphates. Further
488 analysis is needed to characterize the metabolism of dAdo in plant cells and to determine
489 how intracellular dAdo leads to TNL activation in Arabidopsis. Since NLRs of the TIR domain
490 type are also found in animals, our results open the possibility to further investigate the role
491 of TNLs in cell death triggered by dAdo in plants and beyond.

492 In animal systems, it has been shown that following import of dAdo into macrophages,
493 dAdo-mediated toxicity involves conversion of dAdo to dAMP by deoxycytidine kinase
494 (DCK) and adenosine kinase (ADK) activity and signaling via subsequent conversion to the
495 corresponding di- and tri-phosphates by nucleotide kinases and activation of caspase-3-
496 induced apoptosis (Winstel *et al.*, 2018). The absence of caspases in plants and the
497 involvement of a TIR-NLR protein in dAdo-mediated cell death in Arabidopsis strongly
498 suggest that this part of the signaling pathway is not conserved between plants and animals
499 and relies on different regulatory and execution mechanisms that require further
500 investigation. The role of the EDS1 family of immunity regulators, which are genetically
501 required for pathogen resistance and execution of cell death by various TIR-NLRs (Lapin et
502 al., 2020), in ISI-mediated cell death also remains to be investigated, as does the
503 involvement of other ISI-like proteins, given that the dAdo-resistance phenotype of ISI is not
504 complete.

505 In summary, we have uncovered a cellular signaling pathway that responds to extracellularly
506 produced metabolites and links nucleoside transport by an equilibrative nucleoside
507 transporter to cellular activation of the MEP pathway and cell death regulated by the TIR-
508 NLR ISI. The fact that dAdo triggers cell death in several plant species, including a basal
509 lineage, suggests that this pathway is likely conserved and represents an ancient cell death
510 mechanism that is shared for the establishment of plant-endophyte symbiosis. This paves
511 the way for a better understanding of immunometabolism in plant-microbe interactions.

512 **Material and methods**

513 **Fungal strains and cultivation techniques**

514 *S. indica* strain DSM11827 (German Collection of Microorganisms and Cell Cultures,
515 Braunschweig, Germany) was cultured on complete medium (CM) containing 2% (w/v)
516 glucose and 1.5% (w/v) agar as previously described in (Hilbert et al., 2012). Liquid (CM)
517 cultures were incubated from spores at 28 °C and 120 rpm.

518 **Plant lines and Arabidopsis transformation**

519 Seeds of *A. thaliana* ecotype Columbia 0 (Col-0), Col-0^{AEQ} , and Col-0^{AEQ} *dorn1* (Choi et al.
520 2014), SALK lines SALK_034517C (*isi*) and SALK_204257C (*ent3*) were used in the
521 experiments. In addition, Col-0 expressing histone H2B fused to mCherry (H2B:2xmCherry)
522 under the UBQ10 promoter in root cells (Marquès-Bueno et al., 2016) were used in this
523 study. Col-0 transformation was performed using the floral dip method as described in

524 (Nizam *et al.*, 2019) to generate the transgenic lines *35S::SiNucA* and
525 *35S::SiNucA:mCherry* (with and without signal peptide).

526 For *Marchantia polymorpha,* the gemmae of the male Tak1 and female Tak2 gametophytes
527 were used.

528 **Plant growth conditions and fungal inoculation**

529 Surface sterilized seeds were germinated and grown on ½ MS medium (Murashige-Skoog
530 medium, with vitamins, pH 5.7) containing 1% (w/v) sucrose and 0.4% (w/v) Gelrite under
531 short-day conditions (8 h light, 16 h dark) with 130 µmol m^{-2} s^{-1} light and 22 °C/18 °C.
532 Two methods were used for fungal inoculation: 1) 7-day-old seedlings were
533 transferred to ½ MS without sucrose or 1/10 PNM (Plant Nutrion Medium, pH 5.7) plates
534 (15-20 seedlings per plate). 1 ml of water containing $5x10^5$ chlamydospores of *S. indica* was
535 pipetted onto the root and surrounding area. Control plants were inoculated with sterile
536 water. 2) Sterile *A.* thaliana seeds were incubated in 1 ml of water containing $5x10^5$ *S. indica*
537 chlamydospores for one hour and then pipetted onto 1/10 PNM plates.

538 For harvesting, individual roots were thoroughly washed with water, a 4 cm root section was
539 cut 0.5 cm below the shoot, and immediately frozen in liquid nitrogen. Two to three plates
540 of 20 seedlings each were pooled per replicate.

541 **Confocal microscopy**

542 Colonized Arabidopsis roots were treated with 5 µg/ml Wheat Germ Agglutinin-Alexa Fluor
543 488 conjugate (WGA-AF 488, Life Technologies, Thermo Fisher Scientific, Schwerte,
544 Germany) or 1 µM FGB1-FITC of (Wawra et al., 2019) To visualize the fungal cell wall. 250
545 ng/ml 4',6-diamidino-2'-phenylindole dihydrochloride (DAPI) or 500 nM SYTOX Orange (Life
546 Technologies, Thermo Fisher Scientific, Schwerte, Germany) were used as nucleic acid
547 stain.

548 A TCS SP8 confocal microscope (Leica, Wetzlar, Germany) was used for confocal laser
549 scanning microscopy on living cells. AF 488 and FITC were excited with an argon laser at
550 488 nm, and the emitted light was detected with a hybrid detector at 500-550 nm. mCherry
551 and SYTOX orange were excited with a DPSS laser at 561 nm, and the signal was detected
552 with a hybrid detector at 590-660 nm. DAPI was excited with a diode laser at 405 nm, and
553 the emitted light was detected with a hybrid detector at 415-460 nm.

554 **DNA and RNA extraction**

555 DNA was extracted from frozen root or fungal material as described in Wawra et al. 2016.
556 Briefly, approximately 500 mg of ground frozen material was dissolved in 1 ml of CTAB
557 extraction buffer (100 mM TrisHCl pH 7.5, 50 mM EDTA pH 8, 1.5 M NaCl, 2% (w/v)
558 cetyltrimethylammonium bromide, 0.05% (v/v) ß-mercaptoethanol) and homogenized for 10
559 min. 500 µl chloroform:isoamyl alcohol mixture (24:1) was added and the tubes were mixed
560 and centrifuged for 5 min. Ethanol and 1 volume of chloroform:isoamyl alcohol mixture

561 (24:1) were added to the upper phase and centrifuged again. The DNA in the upper phase
562 was precipitated with 1 volume of isopropanol at 4 °C for 1 h.

563 RNA was extracted with TRIzol (Invitrogen, Thermo Fisher Scientific, Schwerte, Germany)
564 and DNA was digested with DNase I (Thermo Fisher Scientific, Schwerte, Germany)
565 according to the manufacturer's instructions. cDNA was synthesized using the Fermentas
566 First Strand cDNA Synthesis Kit (Thermo Fisher Scientific, Schwerte, Germany).

567 **Quantitative RT-PCR analysis**

568 For quantitative real-time PCR, the 2x GoTaq qPCR Master Mix (Promega, Mannheim,
569 Germany) was used. 500 nM forward and reverse primers and 10-20 ng of cDNA or gDNA
570 template were added to each. The reaction was performed in a CFX connect real time
571 system (BioRad, Munich, Germany) with the following program: 95°C 3min, 95°C 15s, 59°C
572 20s, 72°C 30s, 40 cycles and melting curve analysis. Relative expression was calculated
573 using the $2^{-\Delta\Delta CT}$ method (Livak and Schmittgen 2001). All oligonucleotides used can be
574 found in Table S8.

575 ***Serendipita* indica transformation.**
576 *S. indica* protoplasts were transformed using the PEG-mediated transformation system as
577 described in (Wawra *et al.*, 2019).

578 **Nuclease activity test**

579 To assay the nuclease activity of the purified protein, 10 nM *Si*NucA was mixed with 100 ng
580 linearized plasmid, 1 µg gDNA, or 1 µg RNA in buffer (5 mM Tris pH 8, 1 mM $MgCl_2$, 1 mM
581 $CaCl_2$, 0.1% microelement solution (from CM medium)). The mixture was incubated at RT
582 for 1 to 30 min, then loading dye was added and samples were run on a 1-2 % agarose gel.

583 To test nuclease activity in the filtrate of an *S. indica* culture, a 5-day-old CM culture was
584 minced and incubated for an additional 3 days. The culture was filtered through Miracloth
585 (Millipore Merck, Darmstadt, Germany), and 50 µl of culture filtrate was added to linearized
586 plasmid DNA, gDNA, or RNA.

587 ***Si*NucA-HA-His purification**

588 A 7-day-old liquid culture of *S. indica* grown in CM medium was filtered through Miracloth.
589 The mycelium was washed with 0.9% NaCl and minced in fresh CM medium in a mixer
590 (MicrotronR MB550 homogenizer (Kinematica, Lucerne, Switzerland)). The culture was
591 regenerated for two days. Subsequently, the culture was filtered with Miracloth and through
592 a 0.45 µm membrane filter. To this cell-free culture filtrate, 1 mM phenylmethanesulfonyl
593 fluoride (PMSF) was added and the pH was adjusted to pH 7 with 1 M Tris pH 8. Proteins
594 were precipitated with 80% ammonium sulfate. The protein pellet was resuspended in 20
595 mM Tris pH 8. Proteins were separated by size exclusion chromatography (Sephadex G
596 200 column, Hiload 6/600) using a 20 mM Tris pH 8 / 150 mM NaCl buffer. Fractions
597 containing *Si*NucA-HA-His were desalted by dialysis and checked by SDS-PAGE and anti-

598 HA Western blot. The protein was stored in 20 mM Tris pH 8. The identity of the protein was
599 verified by LC-MS/MS.

600 **Purification of proteins and measurement of enzyme kinetics of *Si*E5NT**

601 *Si*E5NT fused to a C-terminal hemaglutinin (HA) and Strep tag (pXCScpmv-HAStrep, V69)
602 was transiently expressed in *Nicotiana benthaminana* and purified by affinity
603 chromatography as described by (Myrach et al., 2017; Werner et al., 2008). Enzyme
604 concentrations were determined using bovine serum albumin standards after SDS-PAGE
605 and Coomassie Blue staining with an Odyssey Fc Dual Mode Imaging System (Li-cor
606 Biosciences, Germany).

607 To determine substrate specificity, different substrates were tested. Briefly, 10 µl of purified
608 enzyme (1.9 x 10^{-4} mg protein) was added to 70 µl of reaction buffer (10 mM MES buffer,
609 pH 6.0; 1 mM $CaCl_2$ and 1 mM $MgCl_2$) and pre-incubated for 5 minutes. Substrates were
610 added (20 µl of a 5 mM stock solution) to give a final reaction volume of 100 µl. The reaction
611 was quenched with 400 µl of MeOH at the indicated times and centrifuged for 10 min at
612 21,000g at 4°C. The supernatant was evaporated in a vacuum concentrator and the dry
613 pellet resuspended in 100 µl of HPLC mobile phase A.

614 Samples were analyzed using an Agilent 1200 SL HPLC system equipped with a diode
615 array detector. 10 µl of the sample was injected onto a Supelcosil LC-18-T column (Sigma-
616 Aldrich) at a flow rate of 0.8 ml min^{-1} and a column temperature of 25°C. The analytes were
617 separated with the following gradient: 0 min, 100% A; 9 min, 100% A; 15 min, 75% A; 17.5
618 min, 10% A; 19 min, 0% A; 23 min, 0% A; 24 min, 100% A; 30 min, 100% A. Mobile phase
619 A consisted of 100 mM KH_2 PO_4 , pH 6.0, in deionized water and mobile phase B consisted
620 of 90% 100 mM KH_2 PO_4 , pH 6.0, in deionized water and 10% MeOH. Appropriate standard
621 solutions were used for quantification. Data were analyzed using Agilent Chemstation
622 software.

623 Kinetic constants for deoxyadenosine monophosphate and adenosine monophosphate
624 were determined using the EnzCheck (Thermo Fisher Scientific, Waltham, USA)
625 phosphatase assay kit according to specifications, using only one-tenth of the
626 recommended reaction volume.

627 **Release of deoxynucleosides from salmon sperm DNA by *Si*NucA and *Si*E5NT.**

628 10 µg of salmon sperm DNA was incubated with 4 µl of *Si*NucA, 10 µl of *Si*E5NT, or a
629 combination of both in a final volume of 40 µl containing 10 mM HEPES, pH 7.2; 100 mM
630 $MgCl_2$; and 1 mM DTT. The enzymes were incubated in the buffer mixture for 5 minutes
631 prior to the addition of DNA. The reaction was incubated at 22 °C for 1 hour and inactivated
632 at 95 °C for 5 minutes. Subsequently, centrifugation was performed at 40000 g and 4 °C for
633 20 minutes. 20 µl of the supernatant was analyzed on a 2% agarose gel. The remaining 20
634 µl of the supernatant was mixed with 50 µl of water and used for HPLC MS/MS analysis.
635 Samples and standards were analyzed using an Agilent 1290 Infinity II HPLC system

636 coupled to an Agilent 6470 triple quadrupole mass spectrometer. Analytes (10 µl samples)
637 were separated on a 50 x 4.6 mm Polaris C18A column (Agilent) using the following
638 gradient: 0 min, 96% A; 8 min, 35% A; 8.2 min, 0% A; 10 min, 0% A; 10.1 min, 96% A.
639 Mobile phase A consisted of 10 mM ammonium acetate, pH 7.5, and mobile phase B was
640 pure MeOH. The flow rate was 0.6 ml min^{-1} and the column temperature was 30°C. In-
641 source parameters were set as previously described for deoxyribonucleoside analysis
642 (Straube et al., 2021). All analytes were measured in positive mode. Transitions (precursor
643 and production), collision energies, and fragmentor energies are listed in Table S9.

644 **PAM fluorometric measurements**

645 PAM fluorometry measurements were performed by transferring 9-day-old Arabidopsis
646 seedlings into 24 well plates containing 2 ml of 2.5 mM MES buffer (pH 5.6). 3 seedlings
647 were pooled in one well. After 24 hours of regeneration, seedlings were treated with
648 solutions of 5' deoxyadenosine (dAdo), adenosine (Ado), or methyl jasmonate (all Sigma-
649 Aldrich, Taufkirchen, Germany), adjusting to a final concentration of 500 µM. Treated
650 seedlings were incubated in complete darkness for 20 min to reach a dark-adapted
651 condition. The photosynthetic activity of the plants was measured using the M-Series PAM
652 fluorometer (Heinz Walz GmbH, Effeltrich, Germany). Data were analyzed using
653 ImagingWin software (v.2.41a; Walz, Germany). When further analysis of photosynthetic
654 area development was required, it was evaluated using Fiji (ImageJ).

655 **Cell death staining with Evans blue**

656 A modified protocol as described in (Vijayaraghavareddy et al., 2017)was used. To quantify
657 cell death induced by *S. indica* in *Arabidopsis*, plants were used for cell death staining at
658 three time points, 7, 10, and 14 days after fungal spore inoculation, using five plants per
659 treatment. For cell death induced by dAdo (or chemically induced cell death), plants were
660 microscoped after 4 days of cell death treatment. To remove external fungal growth or
661 chemical treatment solutions, plants were washed three times in ddH_2O before cell death
662 staining in a 2.5 mM Evans blue solution (Sigma-Aldrich, lot #MKCH7958) dissolved in 0.1
663 M $CaCl_2$ pH 5.6 for 15 minutes. After extensive washing for one hour with ddH_2O, images
664 were captured using a Leica M165 FC microscope.

665 **Activity-based protein profiling**

666 After treatment with 500 µM dAdo, 500 µM Ado, or MES buffer, 9-day-old Arabidopsis
667 seedlings were frozen in liquid nitrogen, ground, and dissolved in 50 mM Tris-HCl buffer
668 (pH 7). After centrifugation, the supernatant was divided and treated with either the
669 proteasome inhibitor MG132 (final concentration: 50 µM, company) or DMSO for 30 min.
670 Samples were then incubated with 26S proteasome probe MVB072 (final concentration: 1
671 µM, company): 1 µM, (Kolodziejek et al., 2010) Samples were then denatured in SDS
672 loading dye at 95 °C and separated on 12% SDS gels. The probe was visualized using the
673 rhodamine settings (excitation: 532 nm, emission: 580 nm) on a ChemiDoc (BioRad, CA,

674 USA). The protein content of the samples was visualized by staining the gel with SYPRO™
675 Ruby (Invitrogen, Carlsbad, CA, USA) according to the manufacturer's instructions.

676 **RNA seq**

677 7-day-old seedlings were transferred from plates to individual wells of 24-well plates
678 containing 0.5 ml of liquid ½ MS medium containing 0.5% (w/v) sucrose. After 5 additional
679 days in liquid culture, the medium was replaced with 1 ml of 500μ M dAdo in 2.5 mM MES
680 buffer pH 5.6 or 2.5 mM MES buffer pH 5.6 alone as a negative control. Three replicates of
681 four seedlings were harvested for each treatment at 0, 3, and 12 h after treatment (hpt),
682 frozen in liquid nitrogen, and stored at -80° C until processing for RNA extraction. Total RNA
683 was extracted using TRIZOL reagent as described above. RNA integrity was confirmed by
684 gel electrophoresis, and quantity and purity were determined using a NanoDrop 2000.
685 Stranded mRNA-seq libraries were prepared according to the manufacturer's instructions
686 (Vazyme Biotech Co., Nanjing, China). Qualified libraries were sequenced on a HiSeq 3000
687 system instrument in the Genomics & Transcriptomics Laboratory at Heinrich Heine
688 University to generate >100 million reads with a read length of 150 bp from three biological
689 replicates. Trimmomatic v. 0.36,(Bolger et al., 2014) was used for quality trimming and
690 adapter clipping. Reads were then mapped to Arabidopsis TAIR10 CDS assembly and
691 quantified using kallisto v. 0.46.2,(Bray et al., 2016), resulting in estimated counts and
692 transcripts per million (TPM) values. The log2 fold difference in gene expression between
693 conditions was estimated using the R packages tximport (Soneson et al., 2015) and
694 DESeq2 (Love et al., 2014). Genes with statistical significance were selected (FDR-adjusted
695 p-value < 0.05). Data have been deposited at NCBI under GEO accession number
696 GSE209761.

697 **Collection of extracellular fluid**

698 7-day-old Arabidopsis seedlings germinated on ½ MS agar containing 1% sucrose were
699 transferred to 24 well plates. Each well contained 3 seedlings in 1.5 ml of 2.5 mM MES and
700 the specific treatment. After transfer, the plants were returned to the growth chamber for
701 three days. The seedlings were then removed and the liquid centrifuged at 4000 g for 15
702 minutes. The supernatant was freeze dried and sent for metabolite analysis.

703 **Metabolite analysis**

704 5 µl of the apoplastic liquid was injected into an Acquity UPLC (Waters Inc.) equipped with
705 a Nucleoshell RP18 column (Macherey & Nagel, 150mm x 2 mm x 2.1µm) using
706 tributylammonium as the ion pairing agent. Solvent A: 10 mM tributylamine (aqueous)
707 acidified with glacial acetic acid to pH 6.2; solvent B acetonitrile. Gradient: 0-2 min: 2% B,
708 2-18 min 2-36% B, 18-21 min 36-95% B, 21-22.5 min 95% B, 22.51-24 min 2% B. Column
709 flow was 0.4 ml min^{-1} throughout. The column temperature was 40 °C. Scheduled metabolite
710 detection based on multiple reaction monitoring (MRM) was performed in negative mode
711 with electrospray ionization (ESI) on a QTrap 6500 (AB-Sciex GmbH, Darmstadt, Germany):
712 Ion source gas 1: 60 psi, ion source gas 2: 70 psi, curtain gas: 35 psi, temperature: 450 °C,

713 ion spray voltage floating: and -4500V). MRM transitions of 189 metabolites covering central
714 carbon and energy metabolism were previously signal optimized and retention times
715 determined (Table S10).

716 **Ca^{2+} influx quantification**

717 Calcium influx assays were performed as previously described in (Wanke et al. 2020).
718 Briefly, individual 7-day-old Arabidopsis seedlings were placed in white 96-well plates filled
719 with 200 µl reconstitution buffer (2.5 mM MES pH 5.7 [Sigma-Aldrich, Taufkirchen,
720 Germany], 10 mM $CaCl_2$ [Roth, Karlsruhe, Germany]). Before incubation overnight in the
721 dark, the solution was replaced with 133 µl reconstitution buffer containing 10 mM
722 coelenterazine (Roth, Karlsruhe, Germany). The following day, chemiluminescence was
723 measured using a TECAN SPARK 10M microplate reader. After baseline measurement, 67
724 µl of three-fold concentrated elicitor solutions (or Milli-Q water as a sham control) were
725 added manually. Cytosolic calcium influx after addition of the trigger was measured
726 continuously for 30 min. To determine the undischarged aequorin for treatment
727 normalization, 100 µl 3 M $CaCl_2$ (in 30% EtOH) was injected into each well, followed by
728 constant measurement for 1 minute. All steps were performed with an integration time of
729 450 msec.

730 **Heterologous protein production in *Nicotiana benthamiana* and protein purification.**
731
732 For heterologous protein production in Nicotiana *benthamiana,* leaves of 4-week-old plants
733 *were* infiltrated with *Agrobacterium tumefaciens* GV3101 strains. *A. tumefaciens* was grown
734 in LB liquid medium with the appropriate antibiotics at 28°C and 180 rpm for 2 days until an
735 OD_{600} of 1 was achieved. Cultures were centrifuged at 3500 rpm for 15 min at RT, the
736 supernatant was discarded and resuspended in 1 ml infiltration buffer (10 mM MES pH 5.5,
737 10 mM $MgCl_2$, 200 µM acetosyringone) and incubated for 1 h in the dark at 28°C, 180 rpm.
738 All strains were diluted with the infiltration buffer to an OD_{600} of 1. Each strain was mixed
739 with P19-expressing strains at a 1:1 ratio. 2-3 leaves per plant were infiltrated with a
740 needleless syringe. After 4 dpi, leaves were separated from the plant and crushed in liquid
741 nitrogen. Protein purification was performed according to (Werner *et al.*, 2008) with minor
742 modifications performed: A 15-ml tube was filled to the 2-ml mark with ground leaf material,
743 and 2 ml of cold extraction buffer (100 mM Tris pH 8.0, 100 mM NaCl, 5 mM EDTA, 0.5%
744 Triton X100, 10 mM DTT, 100 µg/ml avidin) was added. The powder was resuspended by
745 vortexing and then centrifuged at 12000 rpm and 4°C for 10 minutes. The supernatant was
746 transferred to a new tube and 100 µl of Strep-Tactin® Macroprep (50% slurry) was added
747 and incubated for 60 min at 4°C in a rotating wheel. The mixture was centrifuged at 700xg
748 at RT for 30 s and the supernatant was completely removed from the beads. The beads
749 were washed once with 4 ml and two additional times with 2 ml of wash buffer (50 mM Tris
750 pH 8.0, 100 mM NaCl, 0.5 mM EDTA, 0.005% Triton X-100, 2 mM DTT) by centrifugation
751 for 30 s at 700xg and the supernatant was discarded. During the final wash, beads were
752 transferred to a 1.5 ml tube with a low binding level. The beads were either boiled directly
753 for 5 min at 95°C with 6x SDS loading dye to run on an SDS-PAGE, or the proteins were

754 eluted from the beads by adding 100 µl of elution buffer (wash buffer + 2.5 - 10 mM biotin)
755 and incubating at 25°C, >800 rpm for 5 min. Samples were centrifuged at 700xg for 20 s
756 and elution was repeated. Elution fractions were pooled, SDS loading dye was added, and
757 samples were run on SDS-PAGE followed by Western blot.

758 **Ion leakage measurements**

759 The seedlings for measurement of ion leakage were prepared in the same manner as
760 seedlings for PAM fluorometry measurements. Ion leakage was measured with a
761 conductivity meter (LAQUAtwin EC-11; Horiba, Newhampton, UK).

762 **Seed germination test**

763 Sterile Arabidopsis seedlings were transferred into 24-well plates containing 2 ml of 1/10
764 PNM medium. The medium contained either 500 µM dAdo or the same volume of 2.5 mM
765 MES (pH 5.6). Ten seeds were placed in each well and grown under short-day conditions
766 after 2 days of stratification. Seedling growth was monitored by PAM fluorometry.
767

768 **Root length measurements**

769 To evaluate root length, scans of the square plates containing seedlings were analyzed
770 using Fiji (ImageJ) and the length of the primary root was measured.

771 **Oxidative burst assay**

772 Individual 7-day-old Arabidopsis seedlings were transferred to white 96-well plates
773 containing 200 µl reconstitution buffer (2.5 mM MES pH 5.7 (Sigma-Aldrich, Taufkirchen,
774 Germany), 10 mM $CaCl_2$ (Roth, Karlsruhe, Germany) and incubated overnight in the growth
775 chamber. The following day, the buffer was replaced with 133 µl reconstitution solution
776 containing 15 $\mu g ml^{-1}$ horseradish peroxidase (Sigma-Aldrich, Taufkirchen, Germany) and
777 15 µM L-O12 (Wako Chemicals, Neuss, Germany). After 10 min incubation, 67 µL of three-
778 fold concentrated elicitor solutions (or Milli-Q water as a mock control) were added manually
779 to the wells. Measurements were started immediately and chemiluminescence was
780 measured continuously with a TECAN SPARK 10M microplate reader (Tecan, Männedorf,
781 Switzerland) at an integration time of 450 ms.

782 **Acknowledgements**

783 We would like to thank Prof. Jijie Chai and Jane Parker for discussions and reading the
784 manuscript prior to submission. We further want to thank Johana Misas Stadtel for her
785 support during ABPP assays. ND & AZ would like to thank Lisa Madhi, Lisa Leson and Lucia
786 Schmitz for their excellent support in the lab. ND was supported by the International Max
787 Planck Research School (IMPRS) on "Understanding Complex Plant Traits using
788 Computational and Evolutionary Approaches", by the University of Cologne and by the SFB
789 1403 Project ID: 1403-414786233. AZ gratefully acknowledges support from the Cluster of
790 Excellence on Plant Sciences (CEPLAS) funded by the German Research Foundation
791 (DFG) under the Excellence Strategy - EXC 2048/1 - Project ID: 390686111 and SFB 1403

Project ID: 1403-414786233. We further would like to thank the U.S. Department of Energy Joint Genome Institute (https://ror.org/04xm1d337) and Yu Zhang, Sravanthi Tejomurthula, Daniel Peterson, Vivian Ng & Igor Grigoriev for producing sequencing data within the work proposal 10.46936/10.25585/60001292.
CPW gratefully acknowledges support from DFG grant WI3411/8-1. Some of the graphical representations were generated using the online tool BioRender.

References

Antonioli, L., Pacher, P., Vizi, E.S., and Hasko, G. (2013). CD39 and CD73 in immunity and inflammation. Trends in Molecular Medicine *19*, 355-367. 10.1016/j.molmed.2013.03.005.
Bolger, A.M., Lohse, M., and Usadel, B. (2014). Trimmomatic: a flexible trimmer for Illumina sequence data. Bioinformatics *30*, 2114-2120. 10.1093/bioinformatics/btu170.
Bray, N.L., Pimentel, H., Melsted, P., and Pachter, L. (2016). Near-optimal probabilistic RNA-seq quantification. Nature biotechnology *34*, 525-527. 10.1038/nbt.3519.
Brinkmann, V., Reichard, U., Goosmann, C., Fauler, B., Uhlemann, Y., Weiss, D.S., Weinrauch, Y., and Zychlinsky, A. (2004). Neutrophil extracellular traps kill bacteria. Science *303*, 1532-1535. 10.1126/science.1092385.
Chambard, M., Plasson, C., Derambure, C., Coutant, S., Tournier, I., Lefranc, B., Leprince, J.M., Kiefer-Meyer, M.C., Driouich, A., Follet-Gueye, M.L., and Boulogne, I. (2021). New Insights into Plant Extracellular DNA. A Study in Soybean Root Extracellular Trap. Cells *10*. ARTN 69 10.3390/cells10010069.
Choi, J., Tanaka, K., Cao, Y., Qi, Y., Qiu, J., Liang, Y., Lee, S.Y., and Stacey, G. (2014). Identification of a plant receptor for extracellular ATP. Science *343*, 290-294. 10.1126/science.343.6168.290.
D'Haeze, W., De Rycke, R., Mathis, R., Goormachtig, S., Pagnotta, S., Verplancke, C., Capoen, W., and Holsters, M. (2003). Reactive oxygen species and ethylene play a positive role in lateral root base nodulation of a semiaquatic legume. Proceedings of the National Academy of Sciences *100*, 11789-11794. 10.1073/pnas.1333899100.
Deshmukh, S., Huckelhoven, R., Schafer, P., Imani, J., Sharma, M., Weiss, M., Waller, F., and Kogel, K.H. (2006). The root endophytic fungus Piriformospora indica requires host cell death for proliferation during mutualistic symbiosis with barley. Proc Natl Acad Sci U S A *103*, 18450-18457. 0605697103 [pii]
10.1073/pnas.0605697103.
Driouich, A., Smith, C., Ropitaux, M., Chambard, M., Boulogne, I., Bernard, S., Follet-Gueye, M.L., Vicre, M., and Moore, J. (2019). Root extracellular traps versus neutrophil extracellular traps in host defence, a case of functional convergence? Biol Rev Camb Philos Soc *94*, 1685-1700. 10.1111/brv.12522.
Hawes, M., Allen, C., Turgeon, B.G., Curlango-Rivera, G., Tran, T.M., Huskey, D.A., and Xiong, Z.G. (2016). Root Border Cells and Their Role in Plant Defense. Annu Rev Phytopathol *54*, 143-161. 10.1146/annurev-phyto-080615-100140.
Hilbert, M., Voll, L.M., Ding, Y., Hofmann, J., Sharma, M., and Zuccaro, A. (2012). Indole derivative production by the root endophyte Piriformospora indica is not required for growth promotion but for biotrophic colonization of barley roots. New Phytologist *196*, 520-534. 10.1111/j.1469-8137.2012.04275.x.
Horsefield, S., Burdett, H., Zhang, X., Manik, M.K., Shi, Y., Chen, J., Qi, T., Gilley, J., Lai, J.S., Rank, M.X., et al. (2019). NAD(+) cleavage activity by animal and plant TIR domains in cell death pathways. Science *365*, 793-799. 10.1126/science.aax1911.
Kilian, J., Whitehead, D., Horak, J., Wanke, D., Weinl, S., Batistic, O., D'Angelo, C., Bornberg-Bauer, E., Kudla, J., and Harter, K. (2007). The AtGenExpress global stress expression data set: protocols, evaluation and model data analysis of UV-B light, drought and cold stress responses. The Plant Journal *50*, 347-363. https://doi.org/10.1111/j.1365-313X.2007.03052.x.
Kloppholz, S., Kuhn, H., and Requena, N. (2011). A Secreted Fungal Effector of Glomus intraradices Promotes Symbiotic Biotrophy. Curr Biol *21*, 1204-1209. S0960-9822(11)00717-2 [pii]
10.1016/j.cub.2011.06.044.

845 Kolodziejek, I., Misas-Villamil, J.C., Kaschani, F., Clerc, J., Gu, C., Krahn, D., Niessen, S.,
846 Verdoes, M., Willems, L.I., Overkleeft, H.S., et al. (2010). Proteasome Activity Imaging and
847 Profiling Characterizes Bacterial Effector Syringolin A Plant Physiology *155*, 477-489.
848 10.1104/pp.110.163733.
849 Lahrmann, U., Ding, Y., Banhara, A., Rath, M., Hajirezaei, M.R., Doehlemann, S., von Wiren, N.,
850 Parniske, M., and Zuccaro, A. (2013). Host-related metabolic cues affect colonization strategies of
851 a root endophyte. Proceedings of the National Academy of Sciences of the United States of
852 America *110*, 13965-13970. 10.1073/pnas.1301653110.
853 Lahrmann, U., Strehmel, N., Langen, G., Frerigmann, H., Leson, L., Ding, Y., Scheel, D., Herklotz,
854 S., Hilbert, M., and Zuccaro, A. (2015). Mutualistic root endophytism is not associated with the
855 reduction of saprotrophic traits and requires a noncompromised plant innate immunity. New
856 Phytologist *207*, 841-857. 10.1111/nph.13411.
857 Lahrmann, U., and Zuccaro, A. (2012). Opprimo ergo sum-Evasion and Suppression in the Root
858 Endophytic Fungus Piriformospora indica. Molecular Plant-Microbe Interactions *25*, 727-737.
859 10.1094/mpmi-11-11-0291.
860 Lapin, D., Bhandari, D.D., and Parker, J.E. (2020). Origins and Immunity Networking Functions of
861 EDS1 Family Proteins. Annu Rev Phytopathol *58*, 253-276. 10.1146/annurev-phyto-010820-
862 012840.
863 Li, G., Liu, K., Baldwin, S.A., and Wang, D. (2003). Equilibrative nucleoside transporters of
864 Arabidopsis thaliana. cDNA cloning, expression pattern, and analysis of transport activities. The
865 Journal of biological chemistry *278*, 35732-35742. 10.1074/jbc.M304768200.
866 Lo Presti, L., Lanver, D., Schweizer, G., Tanaka, S., Liang, L., Tollot, M., Zuccaro, A., Reissmann,
867 S., Kahmann, R., and Merchant, S. (2015). Fungal Effectors and Plant Susceptibility. In Annual
868 Review of Plant Biology, Vol 66, pp. 513-545. 10.1146/annurev-arplant-043014-114623.
869 Love, M.I., Huber, W., and Anders, S. (2014). Moderated estimation of fold change and dispersion
870 for RNA-seq data with DESeq2. Genome biology *15*, 550. 10.1186/s13059-014-0550-8.
871 Marquès-Bueno, M.M., Morao, A.K., Cayrel, A., Platre, M.P., Barberon, M., Caillieux, E., Colot, V.,
872 Jaillais, Y., Roudier, F., and Vert, G. (2016). A versatile Multisite Gateway-compatible promoter
873 and transgenic line collection for cell type-specific functional genomics in Arabidopsis. The Plant
874 Journal *85*, 320-333. https://doi.org/10.1111/tpj.13099.
875 Mucha, J., Guzicka, M., Ratajczak, E., and Zadworny, M. (2014). Strategies utilized by trophically
876 diverse fungal species for Pinus sylvestris root colonization. Tree Physiol *34*, 73-86.
877 10.1093/treephys/tpt111.
878 Myrach, T., Zhu, A., and Witte, C.P. (2017). The assembly of the plant urease activation complex
879 and the essential role of the urease accessory protein G (UreG) in delivery of nickel to urease. The
880 Journal of biological chemistry *292*, 14556-14565. 10.1074/jbc.M117.780403.
881 Ngou, B.P.M., Ahn, H.K., Ding, P., and Jones, J.D.G. (2021). Mutual potentiation of plant immunity
882 by cell-surface and intracellular receptors. Nature *592*, 110-115. 10.1038/s41586-021-03315-7.
883 Nizam, S., Qiang, X., Wawra, S., Nostadt, R., Getzke, F., Schwanke, F., Dreyer, I., Langen, G.,
884 and Zuccaro, A. (2019). Serendipita indica E5'NT modulates extracellular nucleotide levels in the
885 plant apoplast and affects fungal colonization. EMBO Rep *20*. 10.15252/embr.201847430.
886 Nostadt, R., Hilbert, M., Nizam, S., Rovenich, H., Wawra, S., Martin, J., Kupper, H., Mijovilovich,
887 A., Ursinus, A., Langen, G., et al. (2020). A secreted fungal histidine- and alanine-rich protein
888 regulates metal ion homeostasis and oxidative stress. New Phytol. 10.1111/nph.16606.
889 Oberwinkler, F., Riess, K., Bauer, R., Selosse, M.-A., Weiß, M., Garnica, S., and Zuccaro, A.
890 (2013). Enigmatic Sebacinales. Mycological Progress *12*, 1-27. 10.1007/s11557-012-0880-4.
891 Olvera-Carrillo, Y., Van Bel, M., Van Hautegem, T., Fendrych, M., Huysmans, M., Simaskova, M.,
892 van Durme, M., Buscaill, P., Rivas, S., Coll, N.S., et al. (2015). A Conserved Core of Programmed
893 Cell Death Indicator Genes Discriminates Developmentally and Environmentally Induced
894 Programmed Cell Death in Plants. Plant Physiol *169*, 2684-2699. 10.1104/pp.15.00769.
895 Pham, A.Q., Cho, S.-H., Nguyen, C.T., and Stacey, G. (2020). Arabidopsis Lectin Receptor Kinase
896 P2K2 Is a Second Plant Receptor for Extracellular ATP and Contributes to Innate
897 Immunity1 [OPEN]. Plant Physiology *183*, 1364-1375. 10.1104/pp.19.01265.
898 Plett, J.M., Daguerre, Y., Wittulsky, S., Vayssieres, A., Deveau, A., Melton, S.J., Kohler, A.,
899 Morrell-Falvey, J.L., Brun, A., Veneault-Fourrey, C., and Martin, F. (2014). Effector MiSSP7 of the

900 mutualistic fungus Laccaria bicolor stabilizes the Populus JAZ6 protein and represses jasmonic
901 acid (JA) responsive genes. Proc Natl Acad Sci U S A *111*, 8299-8304.
902 10.1073/pnas.1322671111.
903 Qiang, X., Zechmann, B., Reitz, M.U., Kogel, K.H., and Schafer, P. (2012). The mutualistic fungus
904 Piriformospora indica colonizes Arabidopsis roots by inducing an endoplasmic reticulum stress-
905 triggered caspase-dependent cell death. Plant Cell *24*, 794-809. 10.1105/tpc.111.093260.
906 Rafiqi, M., Jelonek, L., Akum, N.F., Zhang, F., and Kogel, K.H. (2013). Effector candidates in the
907 secretome of Piriformospora indica, a ubiquitous plant-associated fungus. Front Plant Sci *4*, 228.
908 10.3389/fpls.2013.00228.
909 Ragnelli, A.M., Aimola, P., Maione, M., Zarivi, O., Leonardi, M., and Pacioni, G. (2014). The cell
910 death phenomenon during Tuber ectomycorrhiza morphogenesis. Plant Biosystems - An
911 International Journal Dealing with all Aspects of Plant Biology *148*, 473-482.
912 10.1080/11263504.2013.788575.
913 Rich-Griffin, C., Stechemesser, A., Finch, J., Lucas, E., Ott, S., and Schäfer, P. (2020). Single-Cell
914 Transcriptomics: A High-Resolution Avenue for Plant Functional Genomics. Trends in plant
915 science *25*, 186-197. 10.1016/j.tplants.2019.10.008.
916 Saur, I.M.L., Panstruga, R., and Schulze-Lefert, P. (2021). NOD-like receptor-mediated plant
917 immunity: from structure to cell death. Nat Rev Immunol *21*, 305-318. 10.1038/s41577-020-00473-
918 z.
919 Schneider, H.M., and Lynch, J.P. (2018). Functional implications of root cortical senescence for
920 soil resource capture. Plant and Soil *423*, 13-26. 10.1007/s11104-017-3533-1.
921 Soneson, C., Love, M.I., and Robinson, M.D. (2015). Differential analyses for RNA-seq: transcript-
922 level estimates improve gene-level inferences. F1000Research *4*, 1521.
923 10.12688/f1000research.7563.2.
924 Straube, H., Niehaus, M., Zwittian, S., Witte, C.P., and Herde, M. (2021). Enhanced nucleotide
925 analysis enables the quantification of deoxynucleotides in plants and algae revealing connections
926 between nucleoside and deoxynucleoside metabolism. Plant Cell *33*, 270-289.
927 10.1093/plcell/koaa028.
928 Tedersoo, L., Bahram, M., Ryberg, M., Otsing, E., Koljalg, U., and Abarenkov, K. (2014). Global
929 biogeography of the ectomycorrhizal /sebacina lineage (Fungi, Sebacinales) as revealed from
930 comparative phylogenetics analyses. Mol Ecol. 10.1111/mec.12849.
931 Thammavongsa, V., Kern, J.W., Missiakas, D.M., and Schneewind, O. (2009). Staphylococcus
932 aureus synthesizes adenosine to escape host immune responses. J Exp Med *206*, 2417-2427.
933 10.1084/jem.20090097.
934 Thammavongsa, V., Missiakas, D.M., and Schneewind, O. (2013). Staphylococcus aureus
935 degrades neutrophil extracellular traps to promote immune cell death. Science *342*, 863-866.
936 10.1126/science.1242255.
937 Thürich, J., Meichsner, D., Furch, A.C.U., Pfalz, J., Krüger, T., Kniemeyer, O., Brakhage, A., and
938 Oelmüller, R. (2018). Arabidopsis thaliana responds to colonisation of Piriformospora indica by
939 secretion of symbiosis-specific proteins. PLOS ONE *13*, e0209658.
940 10.1371/journal.pone.0209658.
941 Tran, T.M., MacIntyre, A., Hawes, M., and Allen, C. (2016). Escaping Underground Nets:
942 Extracellular DNases Degrade Plant Extracellular Traps and Contribute to Virulence of the Plant
943 Pathogenic Bacterium Ralstonia solanacearum. PLoS Pathog *12*, e1005686.
944 10.1371/journal.ppat.1005686.
945 Vijayaraghavareddy, P., Adhinarayanreddy, V., Vemanna, R.S., Sreeman, S., and Makarla, U.
946 (2017). Quantification of Membrane Damage/Cell Death Using Evan's Blue Staining Technique.
947 Bio-protocol *7*, e2519. 10.21769/BioProtoc.2519.
948 Voß, S., Betz, R., Heidt, S., Corradi, N., and Requena, N. (2018). RiCRN1, a Crinkler Effector
949 From the Arbuscular Mycorrhizal Fungus Rhizophagus irregularis, Functions in Arbuscule
950 Development. Frontiers in Microbiology *9*. 10.3389/fmicb.2018.02068.
951 Wan, L., Essuman, K., Anderson, R.G., Sasaki, Y., Monteiro, F., Chung, E.H., Osborne Nishimura,
952 E., DiAntonio, A., Milbrandt, J., Dangl, J.L., and Nishimura, M.T. (2019). TIR domains of plant
953 immune receptors are NAD(+)-cleaving enzymes that promote cell death. Science *365*, 799-803.
954 10.1126/science.aax1771.

955 Wawra, S., Fesel, P., Widmer, H., Neumann, U., Lahrmann, U., Becker, S., Hehemann, J.H.,
956 Langen, G., and Zuccaro, A. (2019). FGB1 and WSC3 are in planta-induced beta-glucan-binding
957 fungal lectins with different functions. New Phytol. 10.1111/nph.15711.
958 Wawra, S., Fesel, P., Widmer, H., Timm, M., Seibel, J., Leson, L., Kesseler, L., Nostadt, R.,
959 Hilbert, M., Langen, G., and Zuccaro, A. (2016). The fungal-specific beta-glucan-binding lectin
960 FGB1 alters cell-wall composition and suppresses glucan-triggered immunity in plants. Nat
961 Commun *7*, 13188. 10.1038/ncomms13188.
962 Weiss, M., Waller, F., Zuccaro, A., and Selosse, M.A. (2016). Sebacinales - one thousand and one
963 interactions with land plants. New Phytologist *211*, 20-40. 10.1111/nph.13977.
964 Wen, F.S., White, G.J., VanEtten, H.D., Xiong, Z.G., and Hawes, M.C. (2009). Extracellular DNA
965 Is Required for Root Tip Resistance to Fungal Infection. Plant Physiology *151*, 820-829.
966 10.1104/pp.109.142067.
967 Werner, A.K., Sparkes, I.A., Romeis, T., and Witte, C.P. (2008). Identification, biochemical
968 characterization, and subcellular localization of allantoate amidohydrolases from Arabidopsis and
969 soybean. Plant Physiol *146*, 418-430. 10.1104/pp.107.110809.
970 Winstel, V., Missiakas, D., and Schneewind, O. (2018). Staphylococcus aureus targets the purine
971 salvage pathway to kill phagocytes. Proc Natl Acad Sci U S A *115*, 6846-6851.
972 10.1073/pnas.1805622115.
973 Wu, Z., Li, M., Dong, O.X., Xia, S., Liang, W., Bao, Y., Wasteneys, G., and Li, X. (2019).
974 Differential regulation of TNL-mediated immune signaling by redundant helper CNLs. New Phytol
975 *222*, 938-953. 10.1111/nph.15665.
976 Xiao, Y., Savchenko, T., Baidoo, E.E., Chehab, W.E., Hayden, D.M., Tolstikov, V., Corwin, J.A.,
977 Kliebenstein, D.J., Keasling, J.D., and Dehesh, K. (2012). Retrograde signaling by the plastidial
978 metabolite MEcPP regulates expression of nuclear stress-response genes. Cell *149*, 1525-1535.
979 10.1016/j.cell.2012.04.038.
980 Yu, D., Song, W., Tan, E.Y.J., Liu, L., Cao, Y., Jirschitzka, J., Li, E., Logemann, E., Xu, C., Huang,
981 S., et al. (2021). TIR domains of plant immune receptors are 2′,3′-cAMP/cGMP synthetases
982 mediating cell death. bioRxiv, 2021.2011.2009.467869. 10.1101/2021.11.09.467869.
983 Yuan, M., Jiang, Z., Bi, G., Nomura, K., Liu, M., Wang, Y., Cai, B., Zhou, J.M., He, S.Y., and Xin,
984 X.F. (2021). Pattern-recognition receptors are required for NLR-mediated plant immunity. Nature
985 *592*, 105-109. 10.1038/s41586-021-03316-6.
986 Zipfel, C., and Oldroyd, G.E.D. (2017). Plant signalling in symbiosis and immunity. Nature *543*,
987 328-336. 10.1038/nature22009.
988 Zuccaro, A., Lahrmann, U., Gueldener, U., Langen, G., Pfiffi, S., Biedenkopf, D., Wong, P.,
989 Samans, B., Grimm, C., Basiewicz, M., et al. (2011). Endophytic Life Strategies Decoded by
990 Genome and Transcriptome Analyses of the Mutualistic Root Symbiont Piriformospora indica. Plos
991 Pathogens *7*. 10.1371/journal.ppat.1002290.

992

993

994

995

996

997

998

999

1000 **Figures & descriptions:**

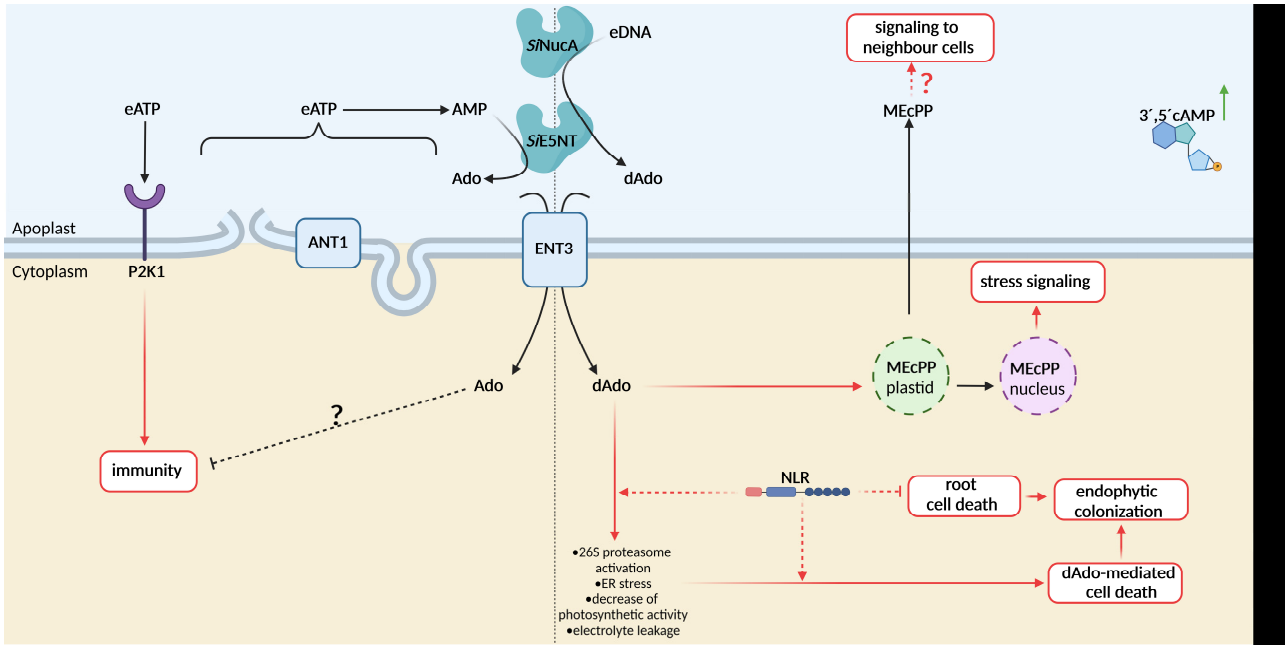

1001

1002 **Figure 1. Current model for dAdo-triggered cell death during colonization of *A.***
1003 ***thaliana* roots by *S. indica.***

1004 The beneficial endophyte *S. indica* secretes two enzymes into the apoplast, the nuclease
1005 *Si*NucA and the ecto-nucleotidase *Si*E5NT. *Si*E5NT is initially involved in manipulating
1006 eATP signaling (left panel), as described in Nizam et al. (2019). *SiNucA* accumulates at the
1007 onset of cell death. The combined activity of *SiNucA* and *SiE5NT* releases
1008 deoxynucleosides from DNA, with a strong preference for dAdo, a potent cell death inducer
1009 in animal systems. dAdo is transported to the cytoplasm *via AtENT3,* where it triggers a cell
1010 death process and contributes to successful fungal colonization. dAdo induces the
1011 production of the retrograde stress signal MEcPP from plastids, activating stress signaling
1012 and possibly intercellular communication. Cell death triggered by dAdo is modulated by an
1013 uncharacterized TIR-type NLR protein (ISI, induced by *S. indica*), providing a link to
1014 immunometabolism.

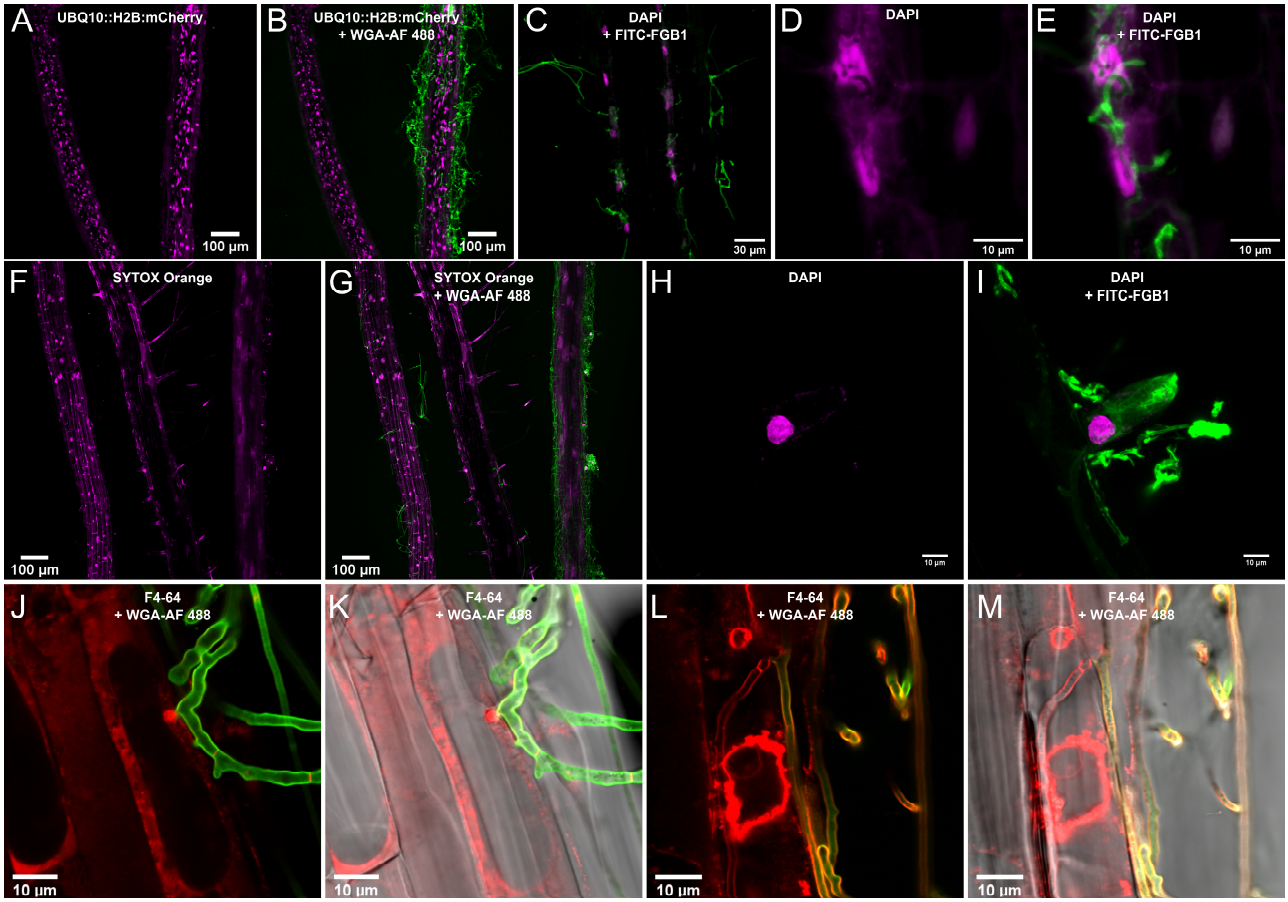

Figure 2. Host cell death during *S. indica* colonization of roots.

(A and B) Arabidopsis roots expressing the fluorescent nuclear marker UBQ10::H2B:mCherry (magenta) stained with the fungal cell wall marker Wheat Germ Agglutinin Alexa Fluor 488 Conjugate WGA-AF 488 (green) at 10 dpi. (C) Plant nuclei stained with DAPI (magenta) and fungal cell wall and matrix stained with the β-glucan binding lectin FGB1-FITC 488 (green) at 6 dpi. As colonization *by S. indica* progresses, host nuclei often become elongated and fade. (D and E) Close-up of *S. indica* hyphae embedded in a host nucleus from (C). (F and G) Staining of nucleic acids of roots colonized with *S. indica* with the dead cell indicator (membrane integrity marker) SYTOX Orange (magenta) and fungal hyphae with WGA-AF 488 (green) at 10 dpi. (H and I) *S. indica* hyphae fluorescently labeled with the β-glucan-binding lectin FGB1-FITC 488 (green) embedded in a DAPI-stained host nucleus (magenta) at 6dpi. (J-M) Progressive vacuolar collapse of colonized root cells. Fungal hyphae are stained with WGA-AF 488 (green), while membranes are stained with FM4-64 (red). (J and K) Initial biotrophic colonization. (L and M) Vacuolar collapse in a dying host cell. CLSM was repeated at least five times with 3 to 4 plants colonized by *S. indica*. Fading of nuclei at the onset of cell death during fungal colonization was regularly observed.

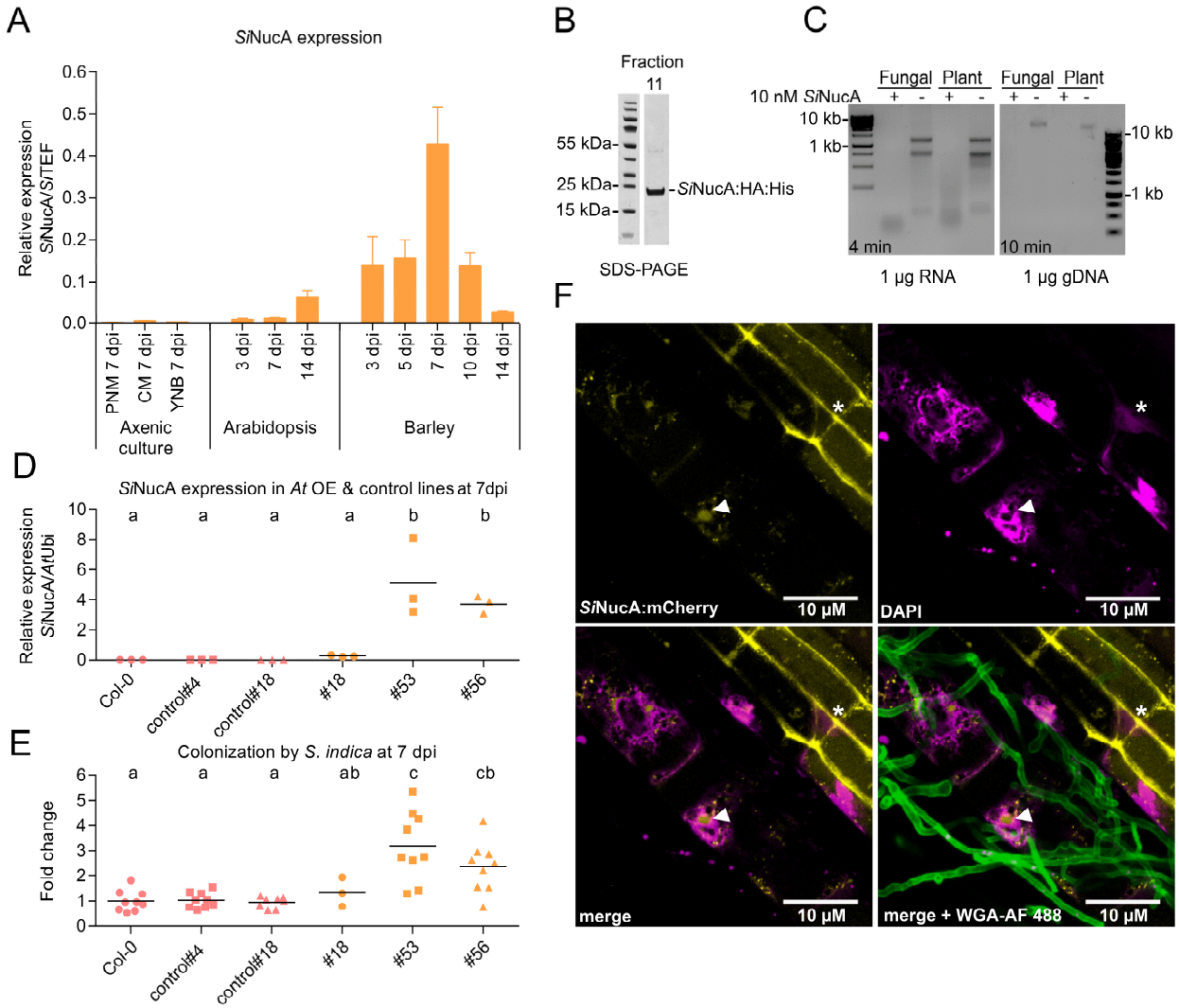

Figure 3. *Si*NucA is a small secreted nuclease involved in fungal accommodation.

(A) *Si*NucA expression in Arabidopsis and barley roots colonized by *S. indica* and axenic cultures measured by the $2^{-\Delta CT}$ method. Error bars: SD, n = 3 (biological replicates). (B) *SiNucA*:HA:His protein enrichment from culture filtrate precipitated with 80% ammonium sulfate and separated by size exclusion chromatography. The resulting fraction was separated by SDS-PAGE and *SiNucA:*HA:His was stained with Coomassie Brilliant Blue. (C) The purified *SiNucA*:HA:His protein was incubated with fungal (*S. indica)* or plant (Arabidopsis) RNA or DNA in 5 mM Tris buffer (pH = 8) containing 1 mM $MgCl_2$ and 1 mM $CaCl_2$ for 4 (RNA) or 10 (DNA) min and visualized after gel electrophoresis. (D) Arabidopsis lines expressing *SiNucA* driven by the 35S promoter (lines 18, 53, and 56) compared with control lines (4 and 18: segregating from T2 generation and Col-0 WT). Roots of plants grown on ½ MS medium were inoculated with *S. indica* and analyzed after 7 dpi. The dots represent independent biological replicates, and the lines represent the mean. Different letters indicate significantly different groups as determined by one-way ANOVA with post-hoc Tukey HSD test ($p<0.05$). (E) Root colonization by *S. indica* in transgenic 35S::*Si*NucA-Arabidopsis lines at 7 dpi was assessed by RT-qPCR by comparing expression of the fungal

housekeeping gene *SiTEF* and the plant gene *AtUbi* and the $2^{-\Delta\Delta CT}$ method, normalized to colonization in the WT Col-0. The dots represent independent biological replicates, while the lines represent the mean. Different letters indicate significantly different groups as determined by one-way ANOVA with post-hoc Tukey HSD test ($p<0.05$). (F) CLSM live cell images of an Arabidopsis root expressing *Si*NucA:mCherry (yellow) and inoculated with *S. indica*. Fungal cell walls are stained with WGA-AF 488 (green) and nuclei with DAPI (magenta). *Si*NucA:mCherry fluorenscence signal accumulates in the apoplast/cell periphery in non-colonized root cells (asterisk) and (re)localizes in host nuclei in colonized cells (arrow).

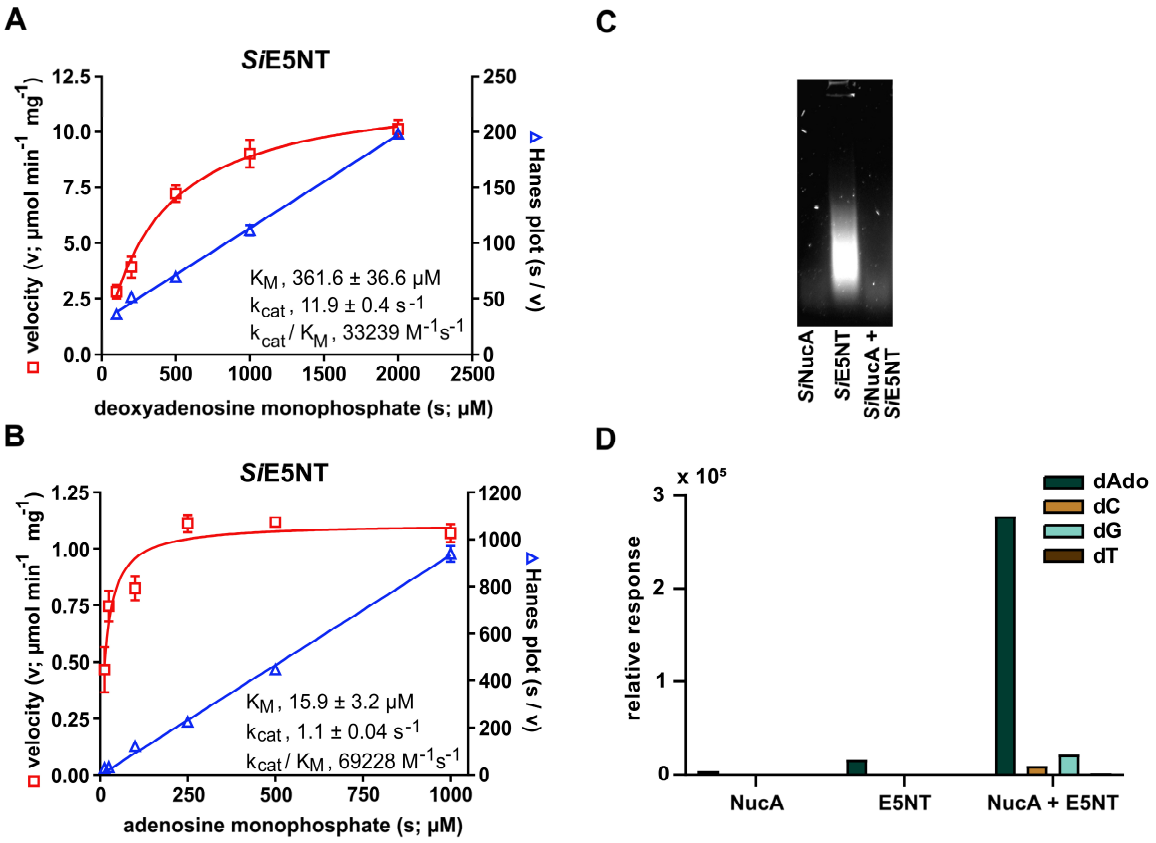

Figure 4. *Si*NucA and *Si*E5NT act synergistically in the production of deoxy nucleosides from DNA.

(A) Enzymatic activity and kinetic constants of *Si*E5NT. Left axis, initial catalytic velocity (v) for phosphate production at different dAMP concentrations fitted with the Michaelis-Menten equation. Right axis, ratio of dAMP concentrations and velocities (s/v) plotted against dAMP concentrations (s) fitted by linear regression (Hanes plot). Error bars: SD, n = 3. (B) As in (A), but using AMP as substrate (n = 3). (C) Degradation of DNA by *Si*NucA and/or *Si*E5NT. 2% agarose gel loaded with the products of a one-hour incubation of 10 µg salmon sperm DNA at 25° C with different enzyme combinations. (D) Relative quantification of dAdo (deoxyadenosine), dC (deoxycytidine), dG (deoxyguanosine) and dT (deoxythymidine)

1070 released during incubation in (C) by HPLC-MS/MS. Deoxynucleotides could not be detected
1071 in any of the reactions.

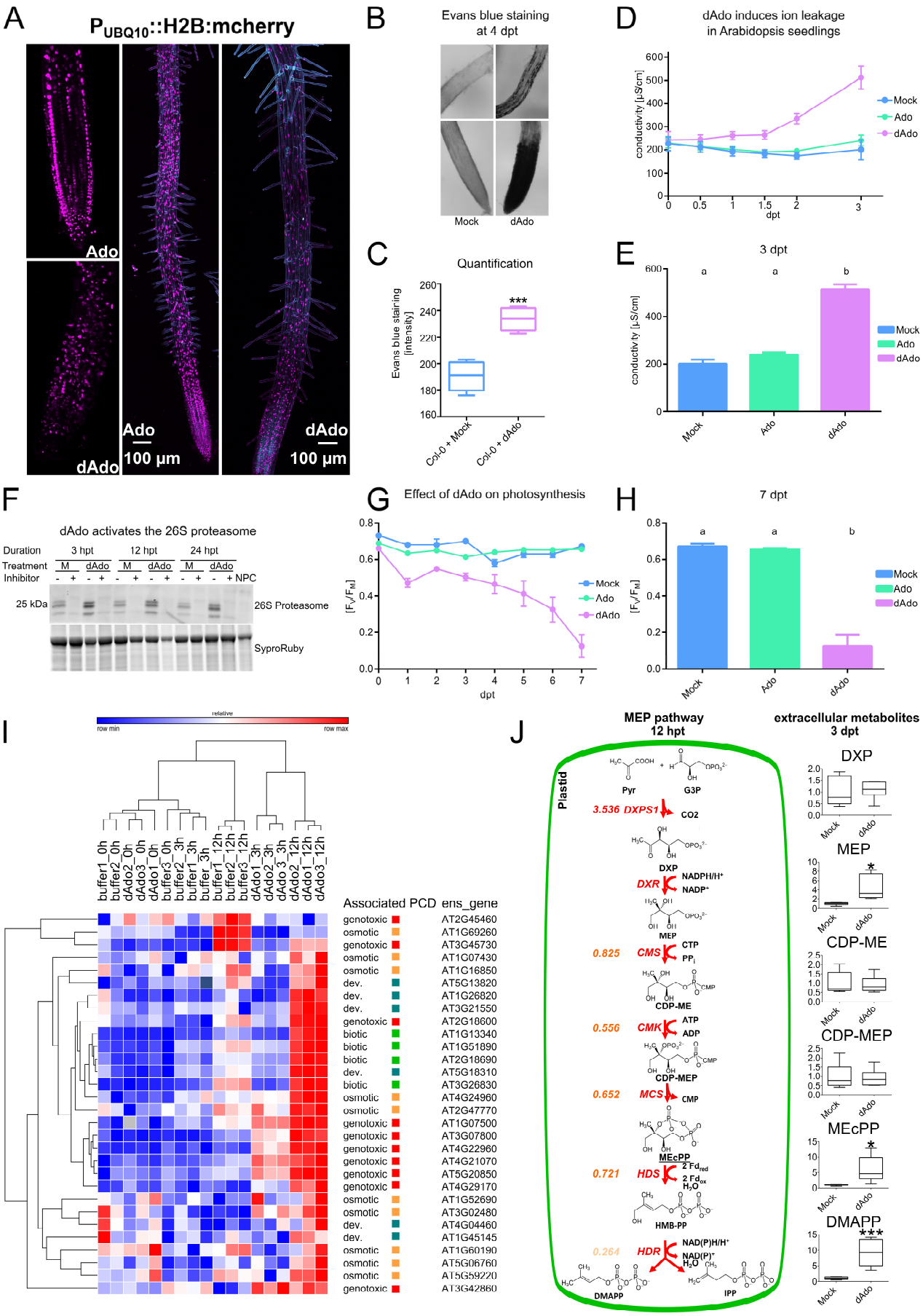
A
P UBQ10::H2B:mcherry
Ado
dAdo
Ado
100 µm
dAdo
100 µm
B
Evans blue staining at 4 dpt
Mock
dAdo
C
Quantification
Evans blue staining [intensity]
***
Col-0 + Mock
Col-0 + dAdo
D
dAdo induces ion leakage in Arabidopsis seedlings
conductivity [µS/cm]
dpt
Mock
Ado
dAdo
E
3 dpt
conductivity [µS/cm]
a
a
b
Mock
Ado
dAdo
F
dAdo activates the 26S proteasome
Duration
3 hpt
12 hpt
24 hpt
Treatment
M
dAdo
Inhibitor
+ NPC
25 kDa
26S Proteasome
SyproRuby
G
Effect of dAdo on photosynthesis
[Fv/FM]
dpt
Mock
Ado
dAdo
H
7 dpt
[Fv/FM]
a
a
b
Mock
Ado
dAdo
I
relative
row min
row max
buffer1_0h
buffer2_0h
dAdo2_0h
dAdo3_0h
dAdo1_0h
buffer3_0h
buffer2_3h
buffer1_3h
buffer_3h
buffer1_12h
buffer2_12h
buffer3_12h
dAdo1_3h
dAdo2_3h
dAdo3_3h
dAdo2_12h
dAdo1_12h
dAdo3_12h
Associated PCD
ens_gene
genotoxic AT2G45460
osmotic AT1G69260
genotoxic AT3G45730
osmotic AT1G07430
osmotic AT1G16850
dev. AT5G13820
dev. AT1G26820
dev. AT3G21550
genotoxic AT2G18600
biotic AT1G13340
biotic AT1G51890
biotic AT2G18690
dev. AT5G18310
biotic AT3G26830
osmotic AT4G24960
osmotic AT2G47770
genotoxic AT1G07500
genotoxic AT3G07800
genotoxic AT4G22960
genotoxic AT4G21070
genotoxic AT5G20850
genotoxic AT4G29170
osmotic AT1G52690
osmotic AT3G02480
dev. AT4G04460
dev. AT1G45145
osmotic AT1G60190
osmotic AT5G06760
osmotic AT5G59220
genotoxic AT3G42860
J
MEP pathway 12 hpt
extracellular metabolites 3 dpt
Plastid
Pyr
G3P
3.536 DXPS1
CO2
DXP
DXR
NADPH/H+
NADP+
MEP
0.825 CMS
CTP
PPi
CDP-ME
0.556 CMK
ATP
ADP
CDP-MEP
0.652 MCS
CMP
MEcPP
0.721 HDS
2 Fdred
2 Fdox
H2O
HMB-PP
0.264 HDR
NAD(P)H/H+
NAD(P)+
H2O
DMAPP
IPP
DXP
MEP
CDP-ME
CDP-MEP
MEcPP
DMAPP
Mock
dAdo

1073 **Figure 5. dAdo induces cell death *in planta.***

1074 (A) CLSM images of seven-day-old Arabidopsis roots expressing the nuclear marker
1075 UBQ10::H2B:mCherry. Incubation with dAdo, but not Ado (500 µM), results in
1076 disorganization of Arabidopsis cells in the root tip and disappearance or fading of nuclear
1077 material. (B) Bright field microscopy of the root tip and differentiation zone of Arabidopsis
1078 seedlings treated with mock/dAdo (500 µM) and stained with Evans blue cell death dye. (C)
1079 Quantification of root cell death in Col-0 root tips 4 days after dAdo treatment. Cell death
1080 was assessed by Evans blue staining. Boxplots show data from 5 biological replicates.
1081 Asterisks represent a significant difference from the mock-treated samples analyzed by
1082 Student's t-test ($p < 0.005$ ***). The experiment was independently repeated 3 times with
1083 similar results. (D) Electrolyte leakage of Col-0 seedlings (9 days old) in MES buffer after
1084 mock, ado or dAdo treatment. Error bars show the standard error of the mean (SEM) from
1085 6 biological replicates. The experiment was independently repeated at least 3 times with
1086 similar results. (E) Electrolyte leakage at 3 dpt of seedlings from (D). Error bars show the
1087 standard error of the mean (SEM) of 6 biological replicates. Different letters indicate
1088 significantly different groups as determined by one-way ANOVA with post-hoc Tukey HSD
1089 test ($p<0.05$). The experiment was independently repeated at least 3 times with similar
1090 results. (F) Activity of the 26S proteasome of Arabidopsis. Total protein extracts from 14-
1091 day-old seedlings treated with 500 µM dAdo or 2.5 mM MES buffer (M) were incubated with
1092 1 µM of probe MVB072 (Kolodziejek et al. 2011). Prior to labeling, samples were incubated
1093 with 50 µM of the proteasome inhibitor epoximycin (+) or DMSO (-). Samples were then
1094 labeled for 2 hours and separated by SDS-PAGE. 26S proteasome activity was visualized
1095 by fluorescence scanning. SYPRO™ Ruby staining was performed to compare sample
1096 amounts. A non-probe control (NPC) consisting of a mixture of all samples incubated with
1097 DMSO was used as an additional control. The experiment was repeated twice with similar
1098 results. (G) Photosynthetic activity (F_V /F_M) of 7-day-old Col-0 seedlings incubated with 500
1099 µM Ado or dAdo. Error bars represent the standard error of the mean (SEM) obtained from
1100 twelve biological replicates. The experiment was repeated three times with similar results.
1101 (H) Photosynthetic activity (F_V /F_M) of 7-day-old Col-0 seedlings incubated with 500 µM Ado
1102 or dAdo at 7 dpt from (G). Error bars represent the standard error of the mean (SEM)
1103 obtained from twelve technical replicates. Different letters indicate significantly different
1104 groups as determined by one-way ANOVA with post-hoc Tukey HSD test ($p<0.05$). (I)
1105 Heatmap of core regulated cell death (RCD) marker-genes expression (selected from
1106 Olvera-Carrillo et al., 2015) of 7-day-old Arabidopsis seedlings after dAdo treatment at 0, 3,
1107 and 12 hours. RNA-Seq data are presented as $\log_2$ (tpm) (Table S6). Heat maps and
1108 hierarchical clustering (one-minus Pearson correlation) were generated using Morpheus,
1109 https://software.broadinstitute.org/morpheus. (J) Graphical representation of the methyl
1110 erythritol 4-phosphate (MEP) pathway. The colored numbers on the left represent the $\log_2$
1111 fold-change after 12 hours of dAdo treatment (Padj < 0.05) as measured by RNA-Seq. The
1112 boxplots on the right show the corresponding extracellular metabolites at 3 dpt. Asterisks
1113 represent significant differences from the mock-treated sample analyzed by Student's t-test
1114 ($p < 0.05$ * ; $p < 0.001$ ***).

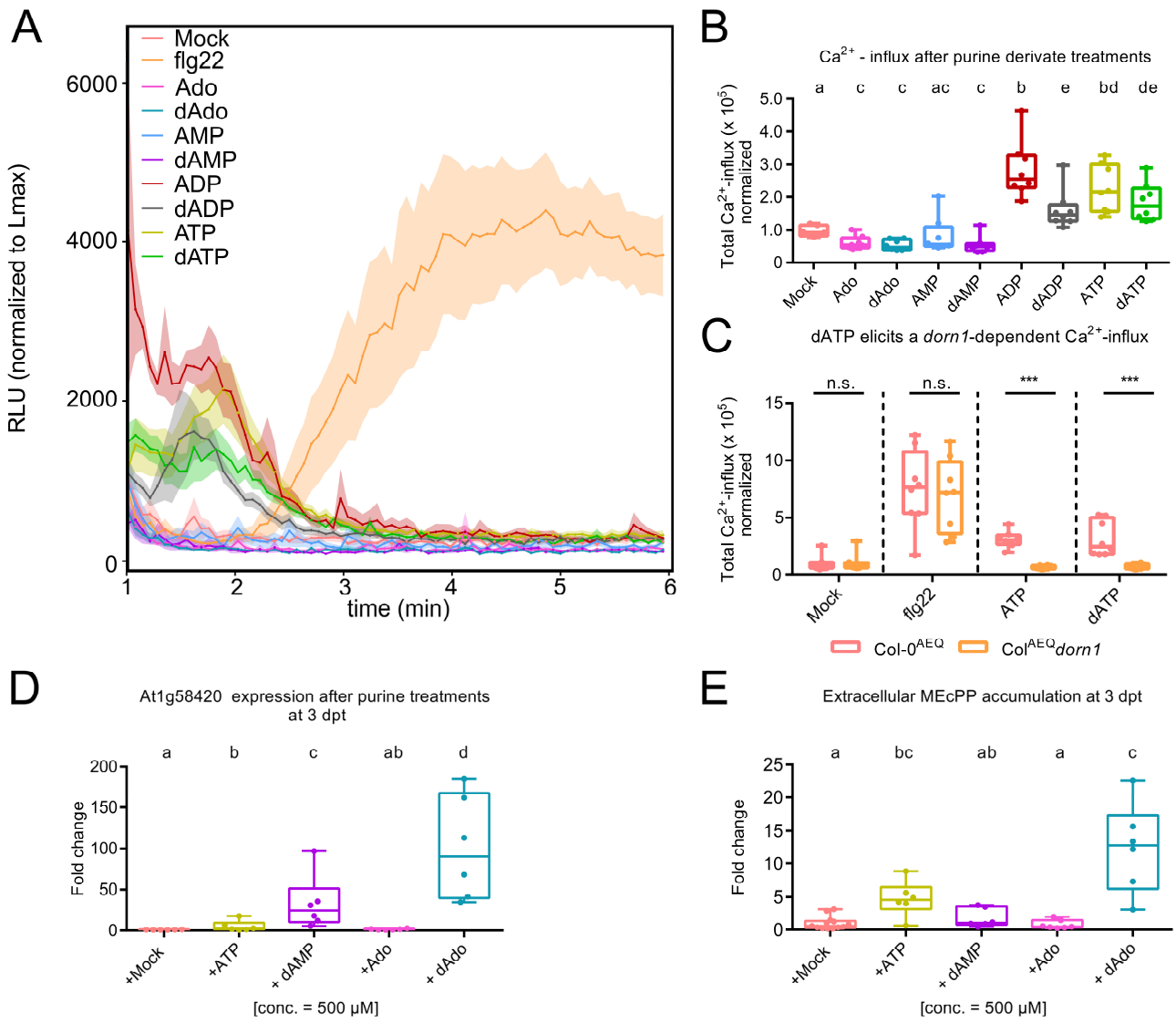

Figure 6. dAdo-triggered signaling and cell death are not mediated by canonical pattern-triggered immune responses.

(A) Ca^{2+} influx after treatment of 7-day-old Arabidopsis Col-0^{AEQ} seedlings with 500 µM purine derivatives dissolved in 2.5 mM MES buffer (pH 5.7). Buffer and 33 µM flg22 were used as positive and negative controls, respectively. Ca^{2+} influx was monitored using a coelenterazine-based chemiluminescence assay and measured as relative light units (RLU). After discharge of the remaining aequorin by addition of $CaCl_2$, the discharge kinetics were integrated and normalized to the maximum Ca^{2+} level. The discharge integral was then used to normalize the kinetics of Ca^{2+} in response to elicitor treatment. The curves represent eight biological replicates, and the experiments were additionally repeated three times independently with similar results. (B) Boxplots show the total Ca^{2+} influx over the measured time period. Calculations were performed as described in (A). Values are means ± SEM of eight biological replicates, each consisting of one seedling. Different letters indicate significant differences as determined by a Kruskal-Wallis test and Dunn's post-hoc test ($p < 0.05$). The experiment was repeated three times with similar results. (C) Comparison of total Ca^{2+} influx in 7-day-old Arabidopsis Col-0^{AEQ} and Arabidopsis Col-0^{AEQ}

dorn1 seedlings after treatment with 500 µM ATP, dATP, 33 µM flg22, or 2.5 mM MES pH 5.7 (mock). Data represent values from eight biological replicates. Calculations were performed as described in (A). Asterisks indicate significant differences between the two genotypes analyzed by Student's t-test ($p < 0.005$ ***). The experiment was repeated three times with similar results. (D) Expression of the marker gene AT1G58420, which responds to wounding and *S.* indica colonization, in treated 7-day-old Col-0 seedlings. Fold change expression was calculated in comparison to the housekeeping gene *AtUbi* and mock treatment using method $2^{-\Delta\Delta Ct}$. Data represent 6 independent biological replicates. Different letters indicate significant differences between groups as determined by Kruskal-Wallis test and post-hoc Wilcox BH adjustment ($p < 0.05$). (E) Metabolic analysis of supernatant from 7-day-old purine-treated Col-0 seedlings at 3 dpt. Points represent data from at least 6 biologically independent replicates normalized to the average of the corresponding mock samples. Different letters indicate significantly different groups as determined by a Kruskal-Wallis test and post-hoc Wilcox BH adjustment ($p < 0.05$).

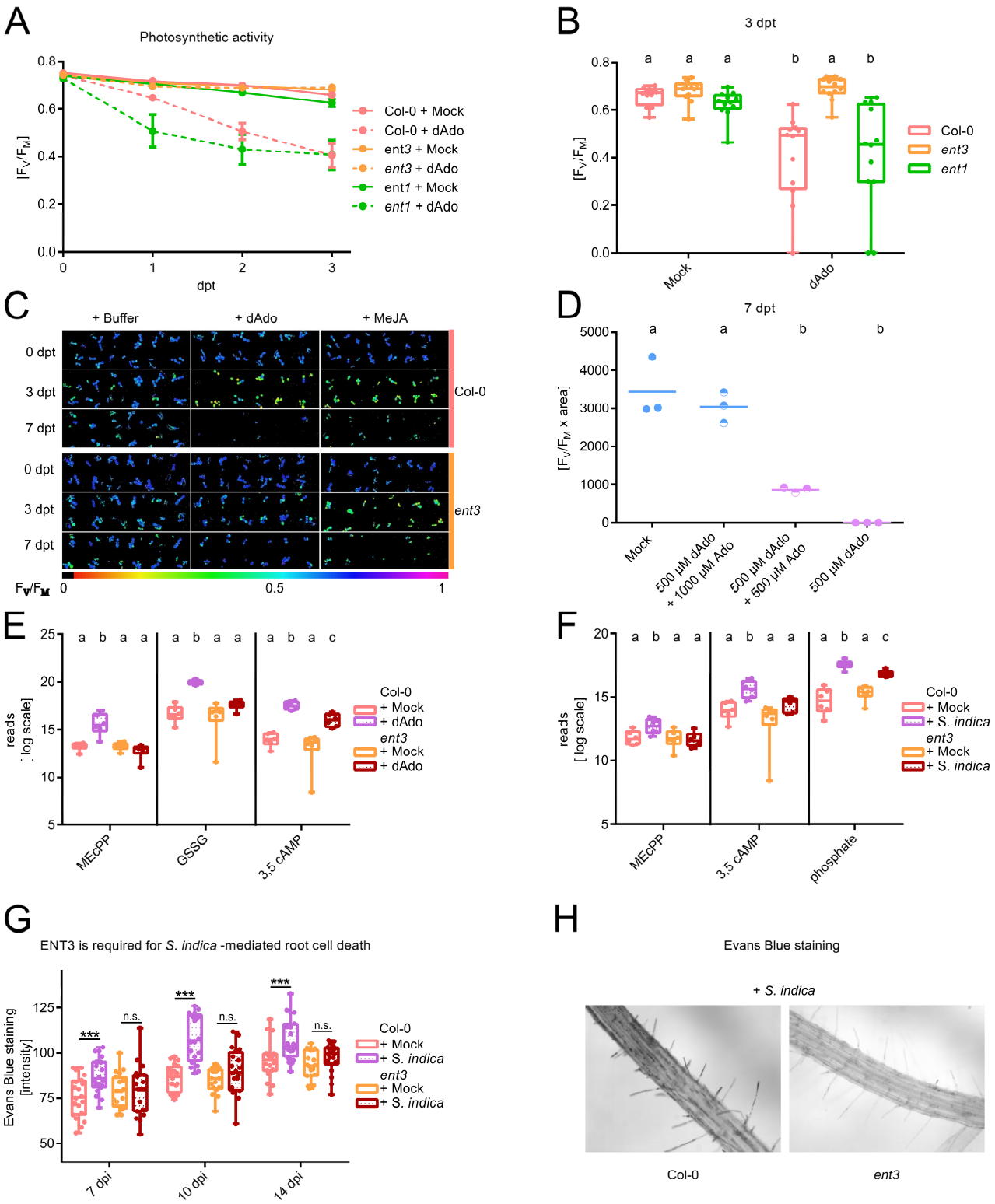

Figure 7. The equilibrative nucleoside transporter ENT3 of Arabidopsis is required for dAdo-mediated signal transduction and cell death.

(A) Photosynthetic activity (F_V /F_M) of 9-day-old mock- and dAdo-treated (500 µM) Col-0, *ent3*, and *ent1* seedlings. Measurements were taken 3 days after treatment (dpt) every 24 hours. Data show the mean and error bars show the standard error of the mean (SEM)

obtained from 12 technical replicates with 3 seedlings each. The experiment was repeated more than three times independently with similar results. (B) F_V /F_M of seedlings from (A) at 3 dpt. Boxplots show data from 12 technical replicates with 3 seedlings each. Different letters indicate significant differences as determined by one-way ANOVA with post-hoc Tukey HSD test ($p < 0.05$). (C) Visualization of F_V/F_M measured by PAM fluorometry. The FV/FM value is visualized by the color scale shown below. Shown are 12 wells with 9-day-old seedlings probed at 0, 3, and 7 dpt with either mock treatment (2.5 mM MES buffer pH 5.6), 500 µM dAdo, or 500 µM MeJA. The experiment was repeated more than three times independently with similar results. (D) Photosynthetic activity (F_V/F_M x photosynthetically active area) of 9-day-old Col-0 seedlings incubated with different concentrations of Ado and dAdo at 7 dpt. Dots represent 3 biologically independent replicates consisting of 12 wells with 3 seedlings each. Different letters indicate significant differences as determined by one-way ANOVA with post-hoc Tukey HSD test ($p < 0.05$). (E) Metabolic analysis of supernatants from 7-day-old Col-0 and ent3 seedlings treated with dAdo at 3 dpt. Boxplots show data from 6 biologically independent replicates. Data are plotted on a log2 scale. Different letters indicate significant differences in measurements of a metabolite as determined by two-way ANOVA with post-hoc Tukey HSD test ($p < 0.05$). (F) Metabolic analysis of the supernatant of 7-day-old Col-0 and *ent3* seedlings *inoculated with S. indica* at different time points after treatment (3′,5′-cAMP: 3 dpi; MEcPP: 6 dpi; phosphate: 10 dpi). Boxplots show data from 6 biologically independent replicates. Data are plotted on a log2 scale . Different letters indicate significant differences in measurements of a metabolite using a two-way ANOVA with post-hoc Tukey HSD test ($p < 0.05$). (G) Quantification of root cell death in 7-day-old Col-0 and *ent3* roots *colonized with S. indica* at 7, 10, and 14 dpi. Cell death was assessed by Evans blue staining. Boxplots show data from 20 biological replicates. Asterisks represent significant differences analyzed by Student's t-test ($p < 0.05$ *, $p < 0.01$ **, $p < 0.005$ ***). The experiment was repeated independently three times with similar results. (H) Evans blue staining of *S. indica-colonized* Col-0 and ent3 roots at 10 dpi. (I) Abundance of *S. indica* in 7-day-old Arabidopsis seedlings. Fungal (*SiTEF*) to plant (*AtUbi)* ratios were calculated using cDNA as template and the $2^{-\Delta CT}$ method. Boxplots represent 6 independent biological replicates. Asterisks indicate a significant difference from Col-0 samples (Student's t-test, $p < 0.05$ *).

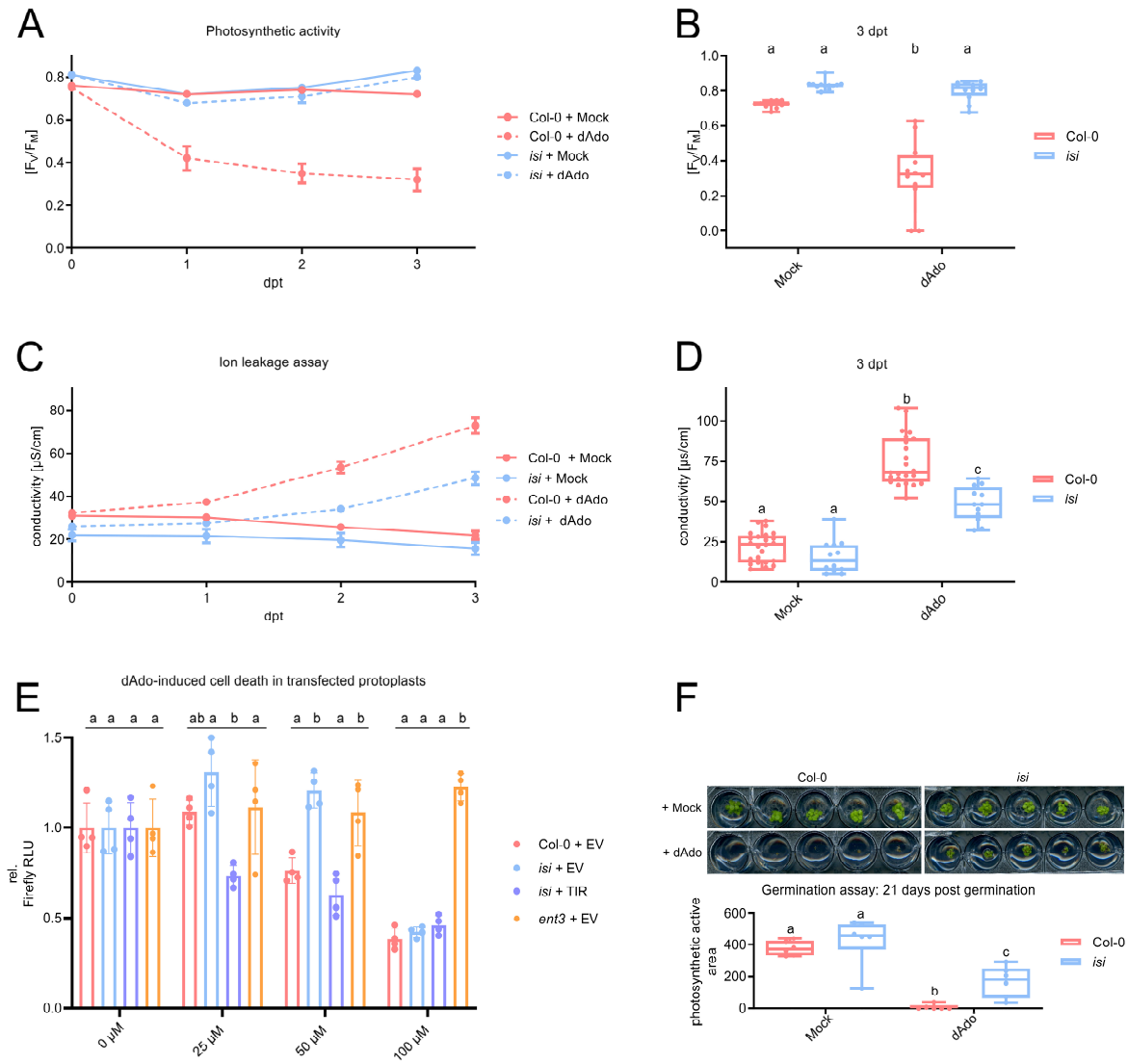

Figure 8. The *At*TIR-NLR AT5G45240 is involved in dAdo-mediated cell death.

(A) F_V /F_M of 9-day-old mock- and dAdo-treated (500 µM) Col-0 and *isi* (AT5G45240 knockout mutant) seedlings. Measurements were performed over 3 days. Data show the mean and error bars show the standard error of the mean (SEM) obtained from 12 technical replicates with 3 seedlings each. The experiment was repeated three times independently with similar results. (B) Boxplots of the measurements of F_V /F_M from (A) at 3 dpt. Different letters indicate significant differences as determined by two-way ANOVA and post-hoc Tukey HSD test ($p < 0.05$). (C) Conductivity of water containing 9-day-old Col-0 or *isi* seedlings 0 - 3 days after mock or dAdo treatment (500 µM). Data points represent the mean, while error bars show the standard error of the mean (SEM) from 12 biological replicates. (D) Boxplots of conductivity measurements from (C) at 3 dpt. Different letters indicate significant differences as determined by two-way ANOVA with post-hoc Tukey HSD test ($p < 0.05$). (E) Relative Luciferase activity of *A. thaliana* protoplasts transfected with Luciferase and either a construct expressing the TIR domain of ISI or an empty vector. Values were normalized to mock treatment (0 µM dAdo). Different letters indicate

significantly different groups as determined by one-way ANOVA with post-hoc Tukey HSD test ($p<0.05$) comparing all protoplast of treatment with one concentration. (F) Germination of Col-0 WT and *isi* seedlings on 1/10 PNM medium containing 500 µM dAdo or MES. The upper half shows photographs of the seedlings after 21 days. The lower half shows the quantification of F_V/F_M measured by PAM fluorometry. Boxplots show F_V/F_M measurements per well, containing six seedlings. Different letters indicate significant differences as determined by two-way ANOVA with post-hoc Tukey HSD test ($p < 0.05$). The experiment was repeated three times independently with similar results.

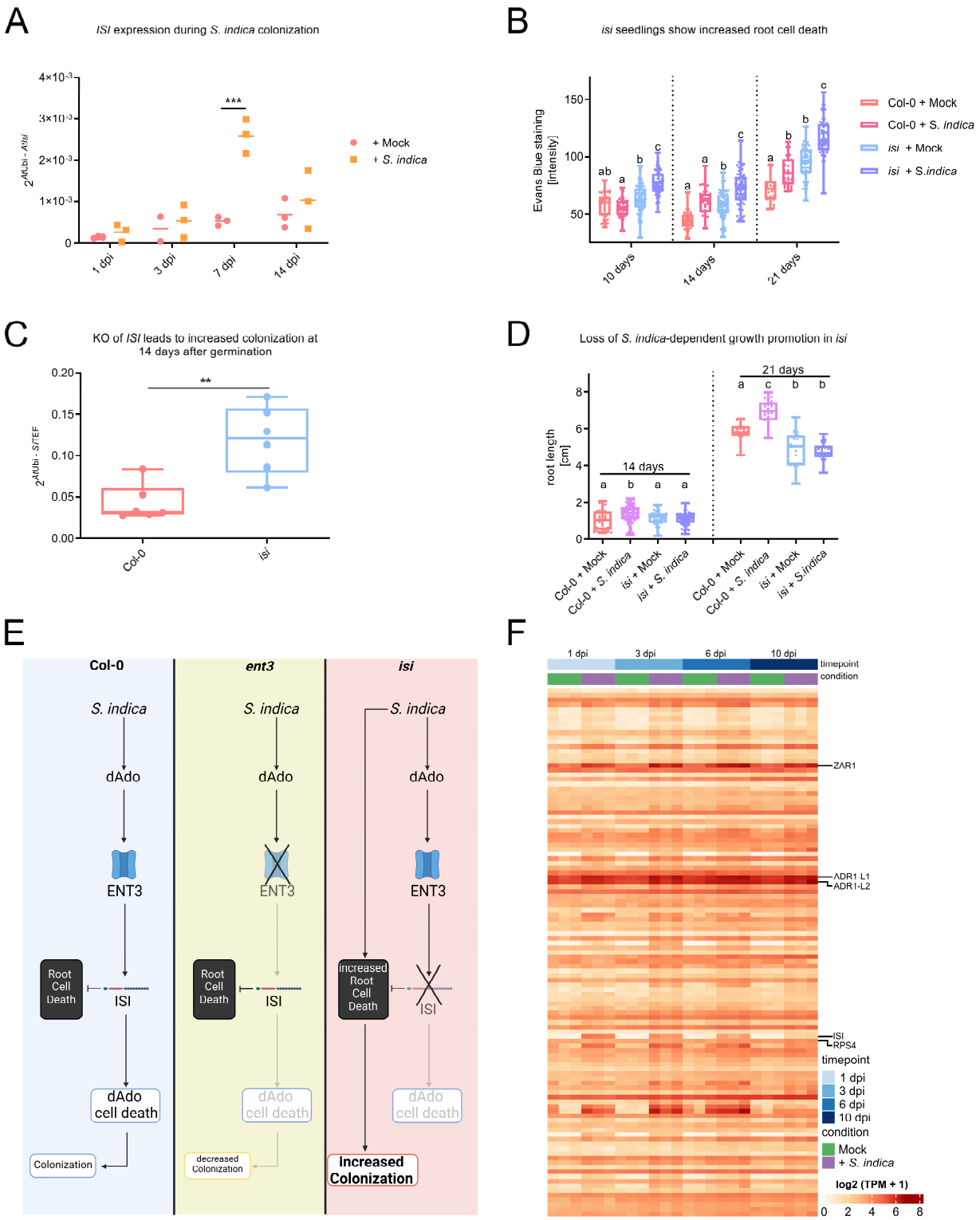

Figure 9. The *At*TIR-NLR AT5G45240 is involved in fungal-mediated growth promotion.

(A) AT5G45240 *(AtISI)* expression in *A. thaliana* roots inoculated with *S. indica* or mock treated. Expression was measured via qRT-PCR and calcuated with the $2^{-\Delta CT}$ method. Data points depict biological replicates and asterisks represent significant differences analyzed

by Student's t-test ($p < 0.005$ ***). (B) Quantification of root cell death in Col-0 WT and *isi* roots colonized by *S. indica* at 10, 14, and 21 days after germination. Cell death was assessed by Evans blue staining. Boxplots show data from 28-80 biological replicates. Different letters indicate significant differences between samples from one time point as assessed by two-way ANOVA with post-hoc Tukey HSD test ($p < 0.05$). (C) Abundance of *S. indica* in Arabidopsis seedlings 14 days after germination. Fungal (*SiTEF*) to plant (*AtUbi)* ratios were calculated using cDNA as template and method $2^{-\Delta CT}$. Boxplots represent 6 independent biological replicates. Asterisks indicate a significant difference from Col-0 WT samples (Student's t-test, $p < 0.01$ **). (D) Root length of Arabidopsis seedlings 14 and 21 days after germination in the presence of *S. indica* or mock treatment. Boxplots show data from 23-86 biological replicates. Different letters indicate significant differences in samples from one time point using two-way ANOVA with post-hoc Tukey HSD test ($p < 0.05$). The experiment was repeated 2 times independently with similar results. (E) Current model illustrating cell death pathways occurring during colonization of *S. indica* in Arabidopsis Col-0 (blue), *ent3* mutant (yellow), and *isi* mutant (red). (F) The heatmap shows the expression values of *A. thaliana* NLR genes with NB-ARC and LRR (NL) domains in *A. thaliana* root samples as log2 transformed TPM values**.** Samples were taken at 1, 3, 6 and 10 days post inoculation with *S. indica* or mock treatment. A more detailed version of the heatmap including an in depth description can be found in Figure S25.